Published in : Journal of Constructional Steel Research (2024), vol. 213, 108355
DOI: 10.1016/j.jcsr.2023.108355
Status : Postprint (Author's version)

SIMPLIFIED METHODS TO PREDICT THE ROBUSTNESS OF STEEL PARKING-STRUCTURE JOINTS

Siyu Xiang [a,b,c], Yongjun He [a,b,*], Tudor Golea [c], Vincent Denoël [c], Jean-François Demonceau [c]

[a] *Key Laboratory of Building Safety and Energy Efficiency of the Ministry of Education, College of Civil Engineering of Hunan University, Changsha 410082, China*
[b] *Key Laboratory for Damage Diagnosis of Engineering Structures of Hunan Province, of Hunan University, College of Civil Engineering of Hunan University, Changsha 410082, China*
[c] *Urban and Environmental Engineering, University of Liege, Liege, Belgium*

KEYWORDS : Steel parking structure ; Structural joint ; Robustness ; Simplified method ; Mechanical models

ABSTRACT

An innovative simplified method for incorporating the behaviour of structural joints in structural analyses of steel parking-structure is proposed in this study. The method is based on the conventional mechanical modelling of joints through special springs that accommodate the arching effect and moment-axial force (*M-N*) interaction. The characterization of these springs in terms of stiffness and resistance is performed using analytical formulae. The accuracy of the proposed method is validated through comparisons to results from advanced numerical methods conducted on a multi-scale approach. Its implementation in sub-structure models is then demonstrated, with the main advantage of extremely reducing the modelling and computational time. Validated sub-structure models are finally employed to investigate the influence of the joint properties on the response of parking structures under vehicle collision scenarios. The results show that considering the rigid and semi-rigid joints in the research are characterised by the welded and bolted connections in the research, for a structure built in a courtyard, bolted connections (semi-rigid joints) are recommended, while for the same structure built near an urban road, welded connections (rigid joints) should be considered to enhance the overall robustness.

1. Introduction

The parking structures investigated in the present paper serve as support frames for automatic mechanical garages, which can take advantage of vertical space to maximise the use of limited land resources in city centres [1]. However, due to the parking function, these structures are at a high risk of collisions. Such collisions can damage the impacted columns, which can induce an overload of the beam end-connections since the load originally carried by the damaged column is redistributed through the activation of alternative load paths [2]. Accordingly, the resistance of the beam-to-column joint at the top of the impacted column needs to be considered in the structural design to avoid a progressive collapse [3].

Published in : Journal of Constructional Steel Research (2024), vol. 213, 108355
DOI: 10.1016/j.jcsr.2023.108355
Status : Postprint (Author's version)

In the past, researchers have carried out numerous experiments on steel frame joints to study their failure mechanisms under extreme loads such as earthquakes [4,5], impacts [6], and column loss [[7], [8], [9], [10], [11]]. These results reveal that, under column loss scenarios, the connections at the beam extremities may be subjected to a compressive arching effect in combination to bending moments. Accordingly, the existing axial force in the beam affects the rotational behaviour of the connection; as the axial force increases, the joints gradually move from a bending-predominant to an axial-predominant loading. In such cases, the axial force in the joint generally exceed 5% of the axial plastic resistance of the beam section [12], which means that, according to EC3 recommendations [13], the joints can no more be modelled as simple rotational spring as the *M-N* interaction as to be accounted for. EC3 follows an existing conventional mechanical model reliant on the plane cross-section assumption, typically utilizing beam elements for analysis. However, this approach lacks precision in predicting the falling joint with a fixed boundary, as it fails to account for the arching effect at the onset of the joint's fall and the *M-N* interaction during the catenary action (refer to Section 3.1 for more details). Detailed numerical methods were used to address this aspect [[14], [15], [16], [17]]. In this regard, the joints are sometimes modelled with solid elements involving considerable modelling effort and computational time to obtain the results. However, reasonable design of the structural joint needs to consider different accidental scenarios and their associated demands, which would in turn require massive computations with such a modelling strategy. Therefore, the use of advanced numerical methods is impractical. Considering this, some simplified methods were proposed in the literature. Izzuddin et al. [18,19] provide a simplified assessment framework for the progressive collapse of a multiple-storey structure. However, this framework assumed all beam-to-column connections as being rigid without taking into account the semi-rigid character of connections [20]. The behaviour of rigid/semi-rigid and full/partial-strength joints under bending and/or axial loads can be predicted using a simplified analytical method called "the component method". The component method is an extension of being based on the conventional model, wherein individual components of connections, such as bolts and plates, are modelled using springs and bars. While it enables efficient calculations and reflects the *M-N* interaction, it does not account for the arching effect. Golea et al. [21,22] used this method to investigate the behaviour of steel joints under different loading conditions and compared the results with experiments demonstrating that the method predicts accurately the joint behaviour. Zhang et al. [23,24] utilized this method to simplify an innovative connection in the steel frame and examine its seismic behaviour while reducing computational costs; the results were in good agreement with the experimental data. The same method is also used in many other research works, such as by Meng et al. [25], D'Antimo et al. [26], and Yan et al. [27] amongst others. Although the component method can reduce the computational cost compared to detailed numerical methods, the characterization of each joint component of the mechanical model can be a tedious process and the implementation of the component method model in structural analysis simulations remains complicated. Therefore, there is a clear need for a method allowing accounting for the joint behaviour in the design of parking structure joints in a simple and accurate way, particularly in capturing the behaviour of *M-N* interaction and arching effects.

Published in : Journal of Constructional Steel Research (2024), vol. 213, 108355
DOI: 10.1016/j.jcsr.2023.108355
Status : Postprint (Author's version)

This paper aims at providing such a simplified method. With the research process shown in Fig. 1, the paper is organized as follows: in Section 2, the characterization of typical joints with typical connections is addressed using a validated finite element (FE) tool. Then, the key properties of the joint connection to be used as data for the proposed simplified method are characterised. Section 3 proposes an innovative simplified method which allows accounting for the arching effect and moment-axial force (*M-N*) interaction. In Section 4, a sub-structure model is developed on the basis of the proposed simplified model, enabling the prediction of the response of the parking structure. In Section 5, the developed model is applied to analyse different impact scenarios on the structure. Based on the results, recommendations are made regarding the joint design.

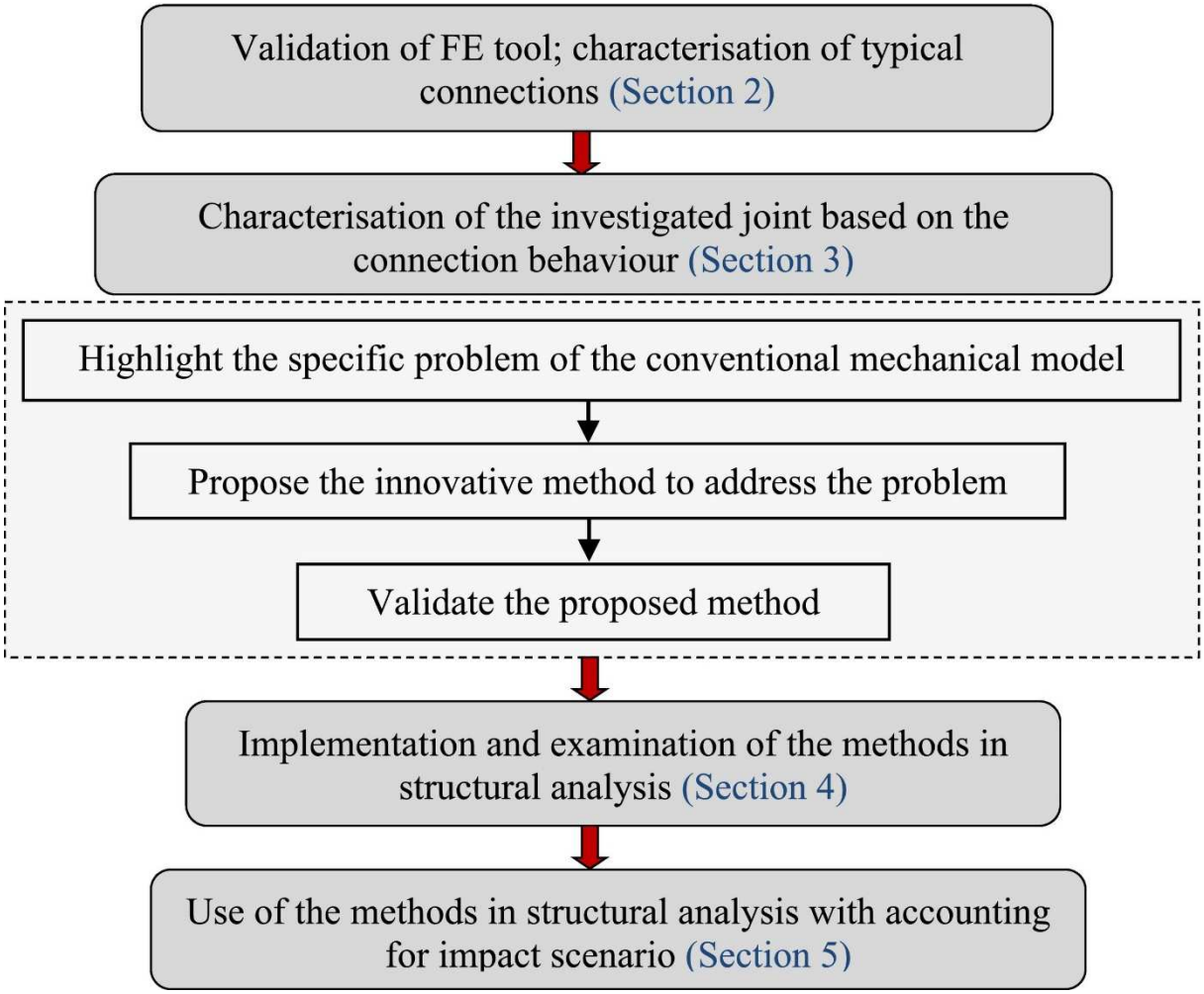

Fig. 1. Research process applied herein.

Published in : Journal of Constructional Steel Research (2024), vol. 213, 108355
DOI: 10.1016/j.jcsr.2023.108355
Status : Postprint (Author's version)

2. Characterization of typical connections in steel parking structures

2.1. TYPICAL SOLUTIONS FOR BEAM-TO-COLUMN JOINTS IN PARKING STRUCTURES

The parking structures within the scope of this paper are shown in Fig. 2 [28]. Typically, the size of such structures is invariable and specifically designed to accommodate private cars, thereby meeting the dimensional requirements of most vehicles. A mobile elevator is located in the middle of the two parking spaces, allowing the lifting and moving of cars. As shown in Fig. 2(b), to be parked, the car is driven into the entrance and then waits to be automatically transferred to the parking space. The columns located at the entrance sides are prone to collisions. When a column is subjected to an impact, it may lose its load-carrying capacity. To avoid the collapse of the structure, the activation of alternative load paths is required and this activation strongly relies on the response of the beam-to-column joint (Fig. 2(c)), the column's base connection, and of the impacted column itself.

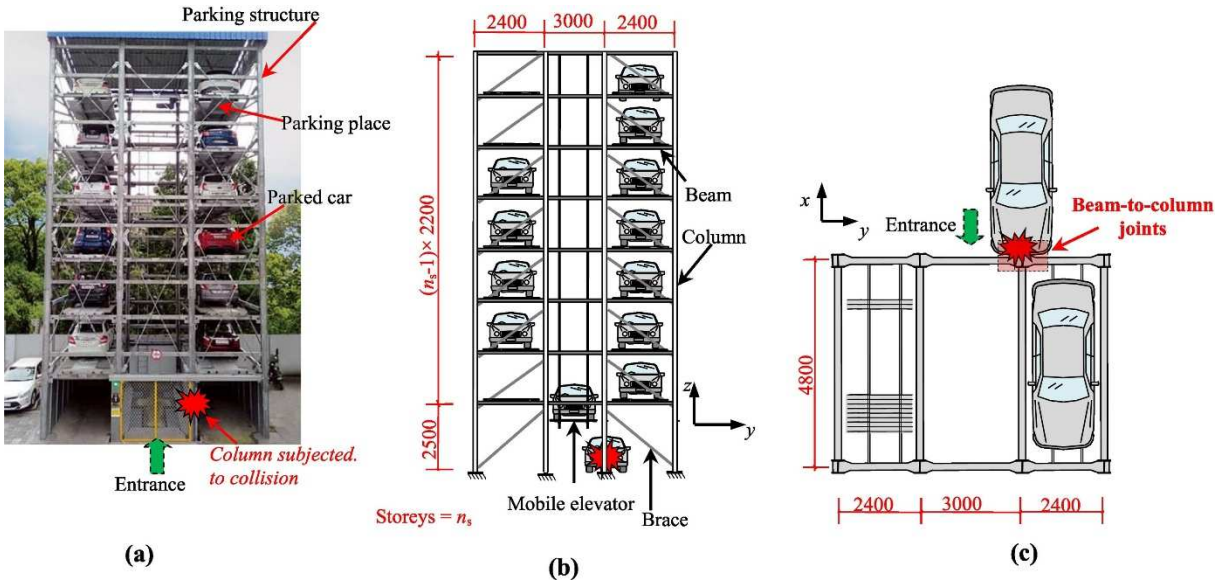

Fig. 2. Configuration of the parking structure: (a) real picture; (b) structural arrangement in elevation view; (c) structural arrangement in top view at the second floor (in mm).

Fig. 3 shows two typical solutions for beam-to-column joints (the rigid and semi-rigid joints) in such parking structures: a welded connection and a bolted connection respectively. For the welded connection, the beam flanges are welded to the column, and the beam web is fixed with two bolts of grade 10.9 (Fig. 3(a)). In the bolted connection, the beam is connected to the column through a transition beam using a bolted end-plate (Fig. 3(b)). Generally speaking, bolted connections are typically easier to assemble than welded connections but offer smaller rotational stiffness [29]. The selection of the connections should consider the specific demands of the parking structures to avoid overdesign. Therefore, these two typical connections will be investigated in this study.

Published in : Journal of Constructional Steel Research (2024), vol. 213, 108355
DOI: 10.1016/j.jcsr.2023.108355
Status : Postprint (Author's version)

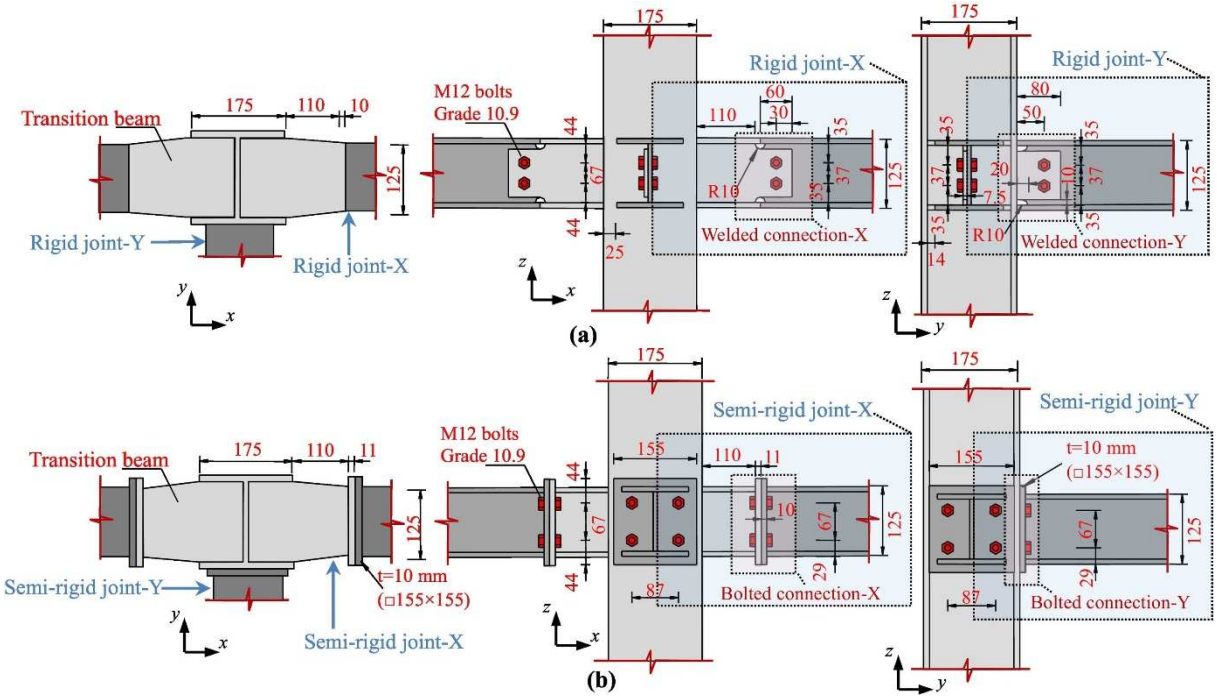

Fig. 3. Typical connections used in the beam-to-column joints: (a) rigid joint; (b) semi-rigid joint (in mm).

2.2. FE MODEL OF THE TYPICAL JOINTS

For the beam-to-column joints, three connections are identified: two along the *x*-direction and one along the *y*-direction. As mentioned before, the details of the different connections present some differences. Consequently, four different connections have been finally extracted in the parking structure, namely welded connection-X, welded connection-Y, bolted connection-X, and bolted connection-Y. The two welded joints are characterised as rigid while the two bolted ones as semi-rigid. Fig. 4 shows FE models of the typical joints, each featuring a typical connection. These models were developed using the ABAQUS/Explicit software [30]. Compared to the ABAQUS/Implicit environment, this one enables faster model calculations, specifically in reflecting material failure and cracks when the required loading time is not extensive. In real-world scenarios, the loss of the column's load-carrying capacity resulting from collisions occurs within a short period, and thus, the loads on the joint may not occur during a completely static process. Consequently, the explicit solver is a better selection for this research. Notably, the purpose of this section is to numerically obtain the mechanical behaviour of these joints.

Published in : Journal of Constructional Steel Research (2024), vol. 213, 108355
DOI: 10.1016/j.jcsr.2023.108355
Status : Postprint (Author's version)

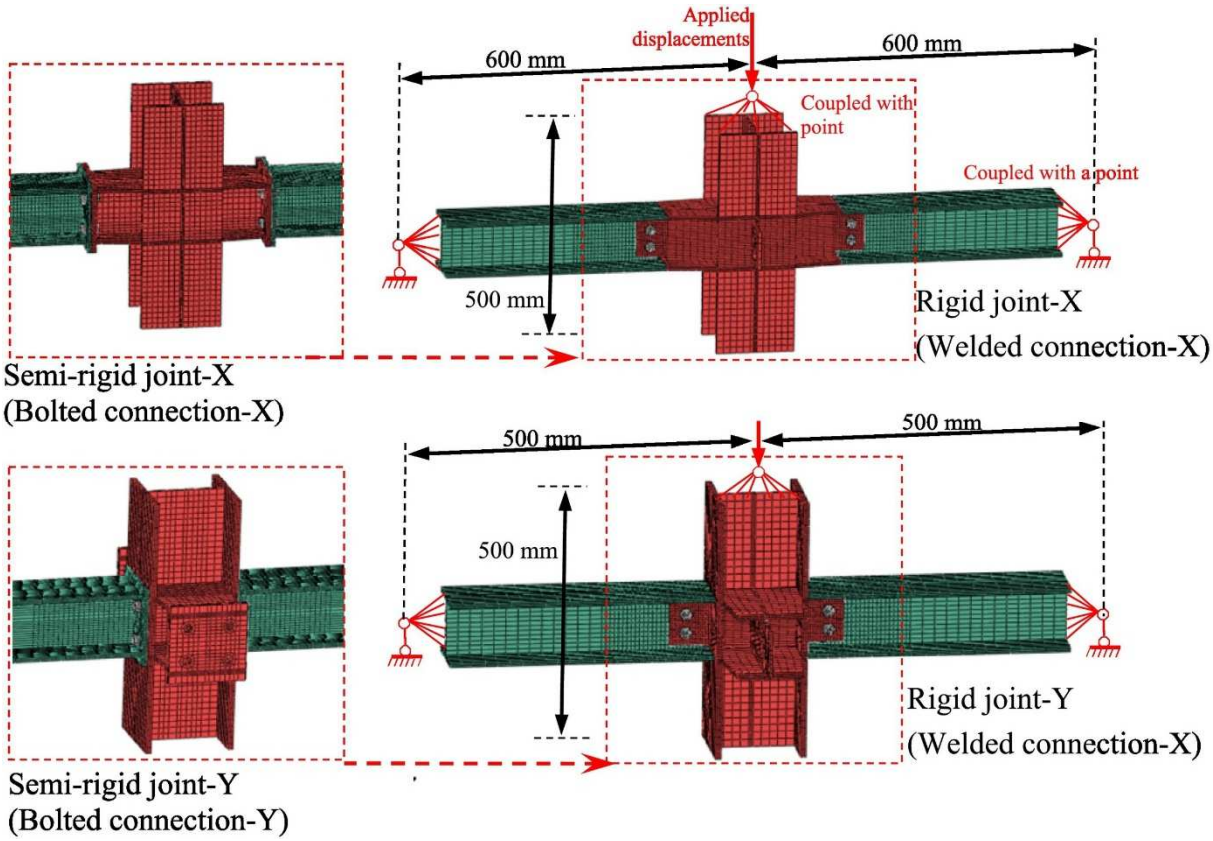

Fig. 4. Finite element models of the typical joints.

All the models shown in Fig. 4 were symmetrical and had a simply supported end. The beam face at the extremities was coupled with a point whose rotational and axial movement was released. Moreover, the column top face was coupled with a point to which a displacement was applied. The applied displacement was defined to increase from 0 to 80 mm with a smooth step amplitude of 0.1 s. It is worth mentioning that before determining the loading time, the influence of the loading time (inertia force) was evaluated at intervals of 0.005 s, 0.01 s, 0.1 s and 0.5 s. The analysis revealed that 0.1 s provides a better balance between the computational cost and accuracy.

According to previous research [31], the "general" contact interaction was used in the numerical model, wherein the normal contact was selected as "hard," and the friction coefficient was set to 0.3. The solid element C3D8R was used for the model. The global mesh size was set to 20 mm, and the zone near the column had a finer mesh size of 8 mm. For the bolts, the mesh size was set to 3 mm. Additionally, three elements were assigned along the thickness of flanges, webs, and plates. The material used for the beam and column was Q235 steel [31], whose material properties are shown in Table 1. A fracture criterion proposed by Bao et al. [32] and Yan et al. [33] was adopted in the FE model to predict the material fracture behaviour. The corresponding parameters were reported and validated in the author's previous research [31]. For the material used for the 10.9 bolts, the ultimate and yield strength were taken as equal to 1005 MPa and 1116 MPa, respectively, and the fracture strain under tension was set to 0.12 according to [34]. In the FE model, it was assumed that damage initiation began at the fracture strain, and linear degradation was defined for the material damage evolution [30,35]. Considering the rapid degradation process when the material reaches the fracture

Published in : Journal of Constructional Steel Research (2024), vol. 213, 108355
DOI: 10.1016/j.jcsr.2023.108355
Status : Postprint (Author's version)

strain as well as the relationship between damage evolution and the element's characteristic length, for simplification, the displacement at failure is defined as a very small value to ensure that the elements are removed upon reaching the fracture strain.

Table 1. Properties of materials used in different numerical model.

Numerical models	**Beam and column**				**Bolt with grade 10.9**		
	***E* (Gpa)**	**f_y (Mpa)**	**f_u (Mpa)**	**ε_u**	**f_y (Mpa)**	**f_u (Mpa)**	**ε_u**
Typical joints	178	274	417	0.25	1005	1116	0.12
BFC and RJ	206	410	542	0.21	1020	1080	/
P1	210	295	418	0.32	1005	1116	0.12

Note: typical joints represent the semi-rigid joint-X, rigid joint-X, semi-rigid joint-Y, and rigid joint-Y as shown in Fig. 3; BFC and RJ correspond to joints used for the model validation (see Section 2.3 and Fig. 4(a)); P1 corresponds to the model as shown in Fig. 4(b); E is the Young's modulus; f_y, f_u, and ε_u represent yield stress, ultimate stress and fracture strain, respectively.

2.3. VALIDATION OF THE FE TOOL

Since, as previously mentioned, the behaviour laws for the materials used for the beams and columns have already been validated by the author [31], this section will focus on the validation of the FE tool (numerical methods). An experimental programme has been reported by Golea et al. [21], where bolted (RJ specimen) and welded (BFC specimen) connection joints were subjected to monotonic bending moments. As the joint types and sizes investigated in this study are similar to those investigated in the present study, the validation of the FE tool can be performed by simulating these tests considering the modelling assumptions described in Section 2.2 and comparing the so-obtained results to the experimental ones. The properties of the materials used in the numerical model are listed in Table 1. The comparisons between numerical and experimental results are shown in Fig. 5(a). With the same vertical displacement, the largest discrepancy of the vertical loads between the simulation and test is 8.0% for BFC specimen, and for RJ specimen, it is −6.4%. The above results demonstrate the accuracy of the FE tool in predicting the response of these joints. It should be mentioned that, for safety reasons, the applied loads on the bolted connection joint (RJ specimen) in the test were small, and thus, the fracture of material in the bolts did not occur. To further examine the reasonability, as an example, the energy relationships in the simulation for BFC specimen are depicted in Fig. 5(b). The kinetic energy (KE) constitutes 4.1% of the total energy (TE), indicating a small influence of the inertia force on the results. Additionally, the artificial strain energy (ASE) is implemented to check the stability and convergence of the analysis, with its low proportion (0.65% TE) demonstrating computational accuracy. In view of further validating the material laws and, in particular, the failure of the joint bolts, another similar experiment (P1) conducted by Kukla et al. [35] was investigated. As illustrated in Fig. 5(c), the load-displacement curves from both the test and the simulation exhibit the same tendency, with a good matching of the crack position and ultimate displacement. Particularly, the failure modes of bolts in the simulation are identical to

Published in : Journal of Constructional Steel Research (2024), vol. 213, 108355
DOI: 10.1016/j.jcsr.2023.108355
Status : Postprint (Author's version)

those in the test. It should be mentioned that the ideally fixed joint boundaries in the simulation differ from the experimental setup where the steel fixing frame is used. The assumed ideally fixed boundaries of the model lead to the stiffness of the load-displacement curve in the simulation that is larger than that of the test.

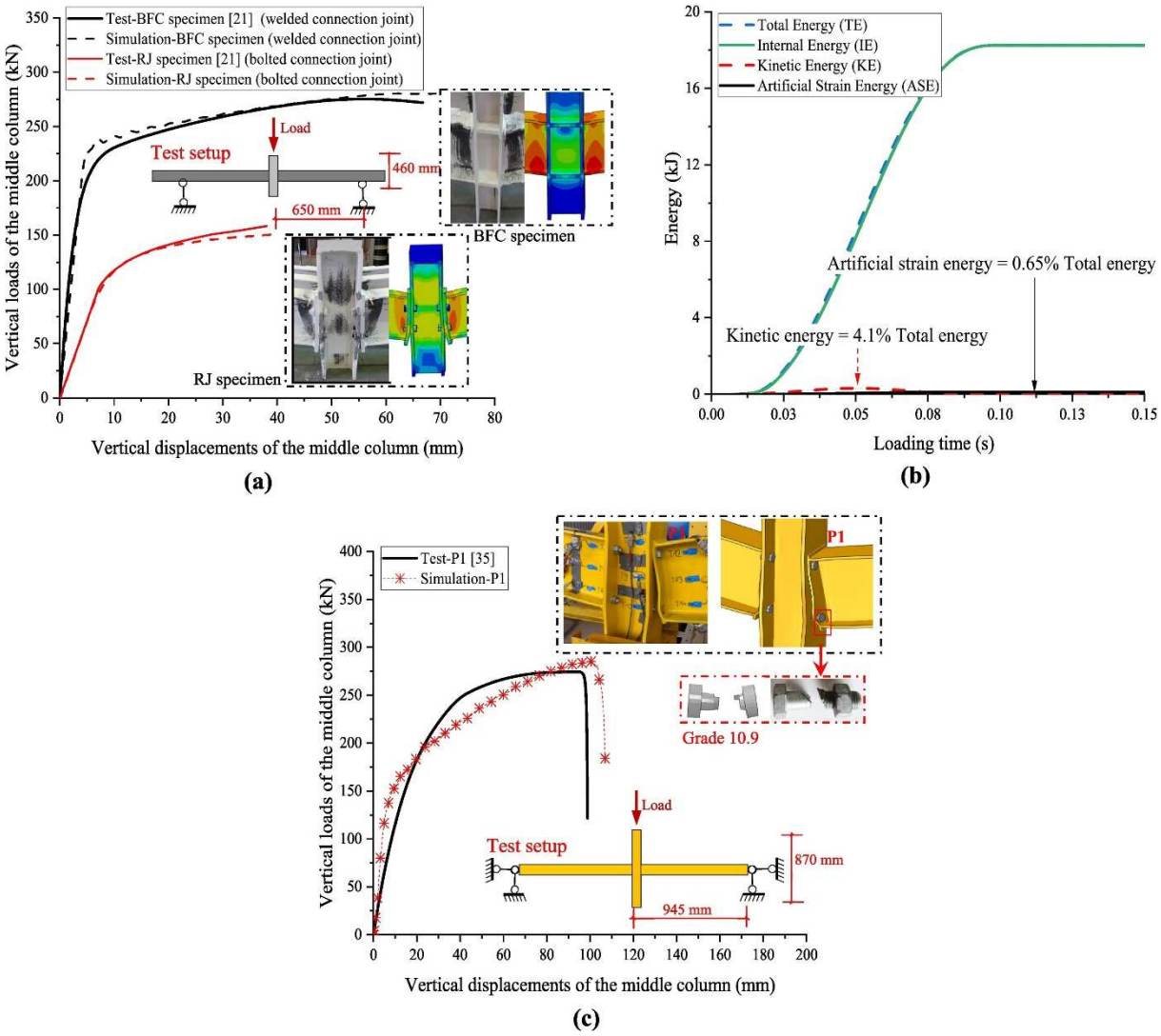

Fig. 5. Validations of FE tool: (a) comparisons of the numerical and experimental results for the welded (BFC) and bolted (RJ) connection joints; (b) the relationship between the different energies in the simulation for BFC specimen; (c) comparisons of the numerical and experimental results of the bolted (P1) connection joint.

In summary, these validations demonstrate that the FE tool (numerical methods) used for predicting the joint behaviour is reliable. The analytical characterization of the investigated joints is performed in the subsequent section.

2.4. CHARACTERIZATION OF THE TYPICAL CONNECTIONS

Fig. 6 displays the numerical results for the typical joints in terms of moment-rotation (M-ϑ) curves and failure modes. From the moment-rotation curves, the joint specimen stiffness $K_j(\vartheta)$ which is the

Published in : Journal of Constructional Steel Research (2024), vol. 213, 108355
DOI: 10.1016/j.jcsr.2023.108355
Status : Postprint (Author's version)

combined contributions of the beam stiffness $K_b(\vartheta)$ and the connection stiffness $K_c(\vartheta)$ can be extracted. Their relationship can be expressed as follows:

$$\frac{1}{K_j(\theta)} = \frac{1}{K_c(\theta)} + \frac{1}{K_b(\theta)} \quad (1)$$

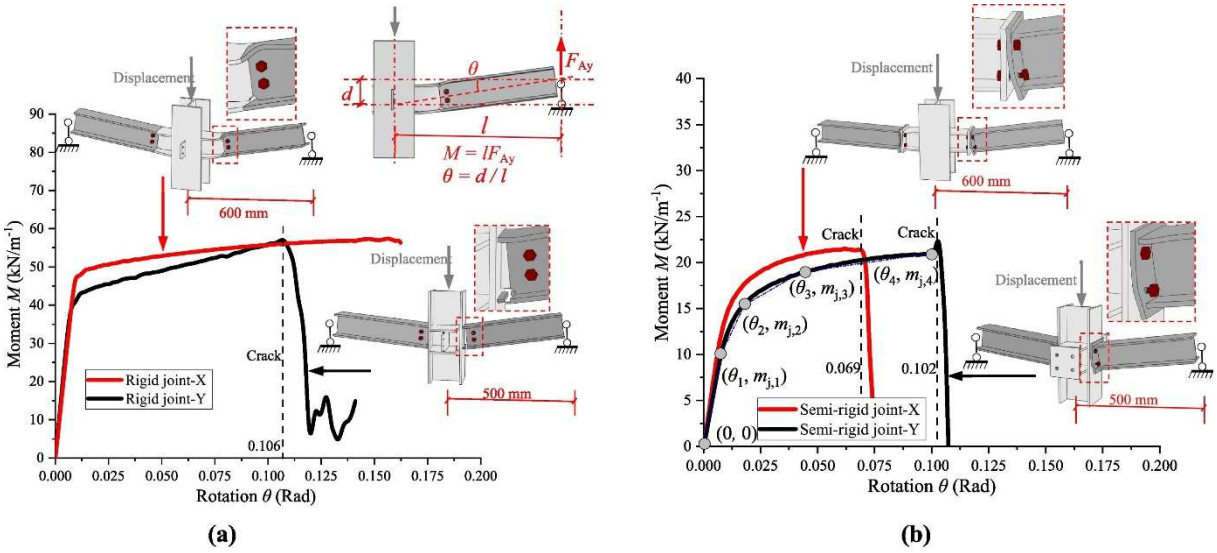

Fig. 6. Moment-rotation relationship of the typical joints: (a) rigid joints; (b) semi-rigid joints.

The purpose of this section is to extract the contribution of the connection from the global joint behaviour.

As shown in Fig. 7, if the joint moment-rotation curve $M_j^{\vartheta}(\vartheta)$ and beam moment-rotation curve $M_b^{\vartheta}(\vartheta)$ are known, the connection moment-rotation curve $M_c^{\vartheta}(\vartheta)$ (or connection moment-vertical displacement curve $M_c^{\vartheta}(d/l)$) can be calculated. The curve $M_j^{\vartheta}(\vartheta)$ has been obtained (Fig. 6). The beam stiffness of the joint can be calculated by treating the beam as a beam with one fixed end and the other simply supported. The material law for the beam is assumed to be bilinear. According to structural mechanics theory, the beam moment-rotation curve $M_b^{\vartheta}(\vartheta)$ can be expressed as follows:

$$M_b^{\theta}(\theta) = \begin{cases} \theta \times 3EI/l^2 & 0 \le \theta < \theta_{beam} \\ k_m \times (\theta - \theta_{beam}) \times 3EI/l^2 + M_{beam} & \theta_{beam} \le \theta \end{cases} \quad (2)$$

where M_{beam} represents the plastic moment of the beam and ϑ_{beam} is the rotational angle corresponding to the plastic moment; EI is the bending stiffness of the beam section; d is the vertical displacement of the joint and l is the length of the beam; k_m is the stiffness reduction factor when the material enters the plastic regime, which is represented by the ratio of elastic stiffness to plastic stiffness and is calculated here as 0.0032.

Published in : Journal of Constructional Steel Research (2024), vol. 213, 108355
DOI: 10.1016/j.jcsr.2023.108355
Status : Postprint (Author's version)

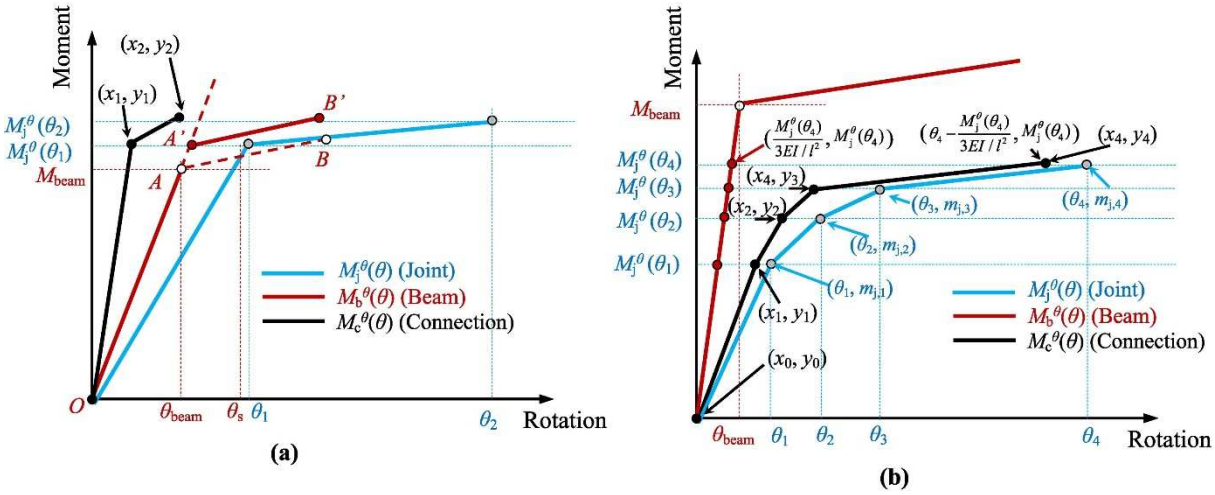

Fig. 7. Generalized relationship of rotational stiffness between the beam, joint and connection: (a) rigid joints and (b) semi-rigid joints.

According to [36], M_{beam} and ϑ_{beam} of the H-shaped section can be calculated as follows:

$$M_{\text{beam}} = f_{\text{y}} b_{\text{f}} t_{\text{f}} \left(h_{\text{w}} + t_{\text{f}}\right) + f_{\text{y}} t_{\text{w}} \left(\frac{h_{\text{w}}}{2}\right)^2 \tag{3}$$

$$\theta_{\text{beam}} = \frac{M_{\text{beam}} l^2}{3EI} \tag{4}$$

where f_y is the yield strength of the material; b_f, t_f, h_w, and t_w are the flange width, flange thickness, web height, and web thickness of the beam section, respectively. It should be mentioned that under the framework of Eq. (3), the contribution from the radius between the flanges and web is ignored.

To determine $M_c^{\vartheta}(\vartheta)$, the coordinates on this curve should be determined in advance. The coordinates on $M_c^{\vartheta}(\vartheta)$ can be obtained considering the following steps:

(1) Extract a sufficient number of points from the curve $M_j^{\vartheta}(\vartheta)$ that adequately represent its shape. As shown in Fig. 6(b), five grey points (ϑ_n, $m_{j,n}$) have been extracted and put into Fig. 7(b).

(2) Depict the curve $M_b^{\vartheta}(\vartheta)$ according to Eq. (2), and then identify the red point whose *y*-ordinates are the same as the blue points reported in Fig. 7(b).

(3) By substracting the *x*-coordinates of the red points from those of the blue points, the black points (x_n, y_n) can be calculated. Fig. 7(b) provides an example calculation for the coordinates of the black point (x_4, y_4).

(4) Using these calculated points (x_n, y_n), the curve $M_c^{\vartheta}(\vartheta)$ can be formulated as follows:

$$M_{\text{c}}^{\theta}(\theta) = k_{\text{j},n}(\theta - x_{n-1}) + y_{n-1} \quad x_{n-1} \le \theta < x_n \tag{5}$$

Published in : Journal of Constructional Steel Research (2024), vol. 213, 108355
DOI: 10.1016/j.jcsr.2023.108355
Status : Postprint (Author's version)

where $k_{j,n}$ is the slope of a line between the two neighbouring points which can be expressed as follows:

$$k_{j,n} = \frac{y_n - y_{n-1}}{x_n - x_{n-1}} \quad (x_0 = 0, y_0 = 0) \tag{6}$$

It should be noted that the curve $M_b^{\vartheta}(\vartheta)$ calculated by Eq. (2) may exhibit slight errors because this equation does not take into account the influence of the transition section (transition beam). In case of bolted connections, such errors are acceptable since the beam stiffness greatly exceeds the joint stiffness. However, in the cases of welded connections (Fig. 7(a)), the calculated beam stiffness may be underestimated and occasionally even falls below the joint stiffness such as the position at the rotation ϑ_s where the red dashed line AB starts to be lower than the blue line $M_j^{\vartheta}(\vartheta)$. This error will cause the calculation of $M_c^{\vartheta}(\vartheta)$ to fail. To address this issue, a modification has been made as shown in Fig. 7(a), where line AB has been shifted to line A'B' along the line OAA'. Not only does this modification enable the calculation of $M_c^{\vartheta}(\vartheta)$, but it also simplifies the definition of the connection stiffness by calculating the two coordinates (x_1, y_1) and (x_2, y_2). Followed by the approach above, the curve $M_c^{\vartheta}(\vartheta)$ can be obtained as shown in Fig. 8 with the corresponding data listed in Table 2.

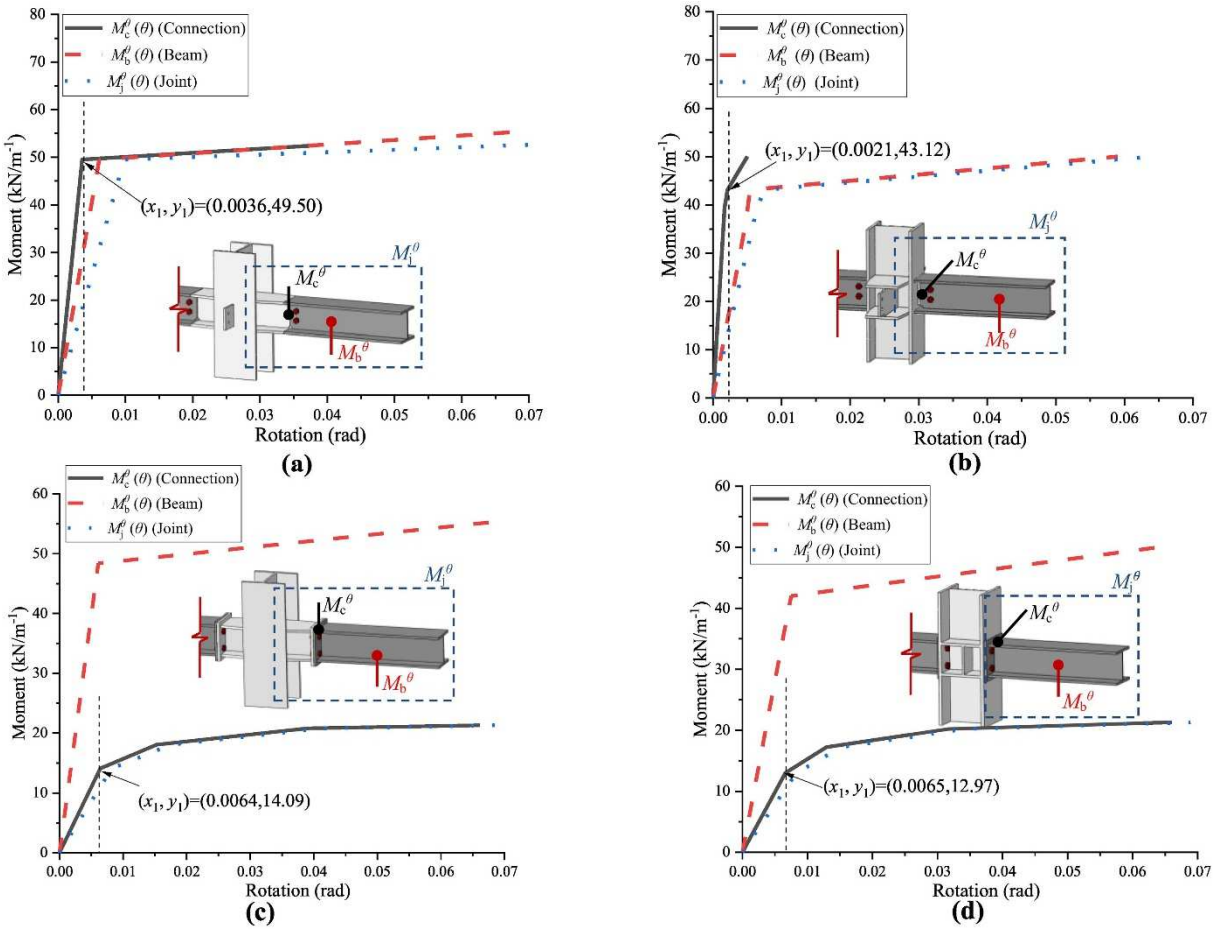

Fig. 8. Calculations of $M_c^{\vartheta}(\vartheta)$ based on $M_b^{\vartheta}(\vartheta)$ and $M_j^{\vartheta}(\vartheta)$: (a) rigid joint-X; (b) rigid joint-Y; (c) semi-rigid joint-X; (d) semi-rigid joint-Y.

Published in : Journal of Constructional Steel Research (2024), vol. 213, 108355
DOI: 10.1016/j.jcsr.2023.108355
Status : Postprint (Author's version)

Table 2. Definitions of the original rotational and axial behaviour on the connections.

Original connection types	**Typical joints**	**(x_1, y_1)**	**(x_2, y_2)**	**(x_3, y_3)**	**(x_4, y_4)**	**k_c^v (N/mm)**
Welded connection-X	Right joint-X	(0.0036, 49.50)	(0.038, 52.5)	/	/	/
Welded connection-Y	Right joint-X	(0.0021, 43.12)	(0.005, 50.10)	/	/	/
Bolted connection-X	Semi-rigid joint-X	(0.0064, 14.09)	(0.0156, 18.06)	(0.0389, 20.86)	(0.066, 21.3)	11,280
Bolted connection-Y	Semi-rigid joint-Y	(0.0065, 12.97)	(0.0130, 17.26)	(0.0319, 20.17)	(0.066, 21.2)	10,840

Note: the units of x_n and y_n are rad and kN/m^{-1} (n = 1 to 4), respectively, and they are coordinates on the M_c^{ϑ} (d); k_c^v is the axial stiffness of the connection; k_c^v of welded connection is extremely large and regard as infinite in the research.

The characterization of the connection behaviour also needs to account for the axial stiffness, especially for the semi-rigid joint. The connection axial stiffness is assumed to be linear. To this end, the connection axial stiffness k_c^v was separated from the joint axial stiffness k_j^v (obtained by numerical results) through a similar principle (Eq. (1)). The result is listed in Table 2. After conducting the aforementioned implementations, the mechanical behaviour of these connections has been determined, providing a preliminary condition for subsequent research on joints with more complex boundary conditions.

3. Characterization of investigated joints through innovative simplified methods

3.1. INTRODUCTION

In the previous section, the rotational and axial stiffness of the investigated connections were obtained. To predict the response of joints, the connection properties ($M_c^{\vartheta}(\vartheta)$ and k_c^v) were directly assigned to the rotational and horizontal springs (S_r and S_h) in the conventional mechanical model as shown in Fig. 9(a). For this model the following assumptions were made: (1) the beam model follows the plane cross-section assumption; (2) the rotational and axial stiffness of the connection are considered as uncoupled; (3) the stain hardening of the steel material is disregarded. Generally, this method yields reliable results only when the joint has a simply supported end such as shown in Fig. 9(c), i.e. when there is no axial force. If the analysed system is axially restrained, the method tends to provide inaccurate results, which is attributed to the arching effect developing in the beams of the subassembly which cannot be accounted for using beam elements and moment-axial force

Published in : Journal of Constructional Steel Research (2024), vol. 213, 108355
DOI: 10.1016/j.jcsr.2023.108355
Status : Postprint (Author's version)

(*M-N*) interaction at the joint level as uncoupled rotational springs are used. This section aims at providing a solution to the aforementioned problems. Specifically, the resistance mechanism of the joint in a column loss scenario will be analysed and then, an innovative simplified method based on conventional models is proposed.

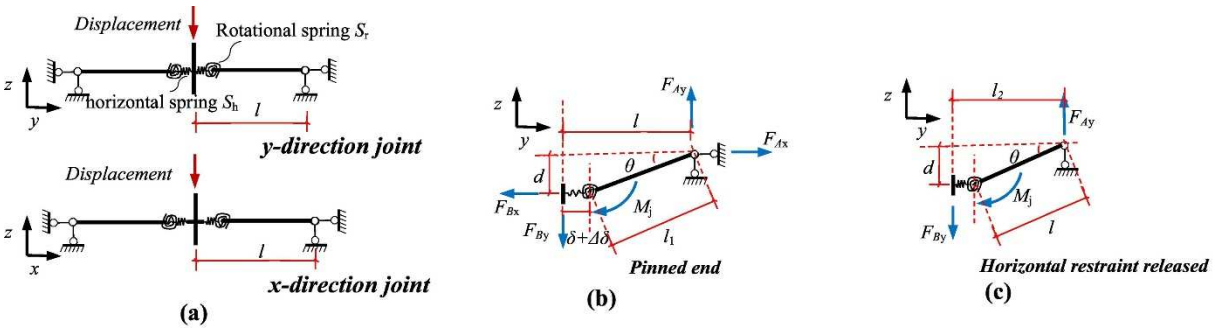

Fig. 9. Conventional mechanical models of the joints: (a) the models of the *x*-direction and *y*-direction joints; (b) the isolated body of the *y*-direction joint under a specific displacement; (c) the isolated body of the *y*-direction joint with horizontal restraint released.

3.2. PHENOMENA OCCURRING IN COLUMN LOSS SCENARIOS

As reported in [[36], [37], [38]], a joint with a large horizontally restraining stiffness is accompanied by considerable influence of the arching effect and *M-N* interaction. To better illustrate this, the horizontal restraining stiffness at the beam extremities was fixed as infinite as shown in Fig. 9(a) and thus the two horizontal restrains were released. As a first step, the *y*-direction joint will be investigated in detail as an example to demonstrate the response of the joint.

Fig. 9(b) shows the *y*-direction joint in isolation. δ represents the length of the horizontal spring S_h, which is taken as zero; $\Delta\delta$ represents the elongation of the horizontal spring when the joint is deforming. Considering force equilibrium on the deformed shape and taking the rotational spring as a moment centre, the force relationship is as follows:

$$F_{Ay}l = M_j + F_{Ax}d \Rightarrow F_{Ay} = \frac{M_j}{l} + \frac{F_{Ax}d}{l} \quad \text{(Pinned end)} \tag{7}$$

where F_{Ay} is the vertical reaction force; M_j is the joint bending moment; F_{Ax} is the horizontal reaction force; d is the vertical displacement.

By treating each term of the equation independently, Eq. (5) can be rewritten as follows:

$$F_{Ay} = \frac{M_j}{l} + \frac{F_{Ax}d}{l} \Rightarrow P = M + C \quad \text{(Pinned end)} \tag{8}$$

In Eq. (6), P represents the vertical load on the column top while the two other terms represent the flexural contribution (M) and catenary action (C) respectively. The former is influenced by the joint bending moment (M_j) and the latter is affected by the horizontal reaction force (F_{Ax}).

Published in : Journal of Constructional Steel Research (2024), vol. 213, 108355
DOI: 10.1016/j.jcsr.2023.108355
Status : Postprint (Author's version)

Because F_{Ay} and F_{Ax} can be directly obtained by detailed numerical analyses, P and C can be calculated. Then, based on Eq. (6), M can be derived. It should be mentioned that M represents the flexural contribution under the influence of *M-N* interaction.

Fig. 9(c) shows the *y*-direction joint whose horizontal restraint is released. In this condition, Eq. (5) can be adapted as follows:

$$F_{Ay} l_2 = M_j \Rightarrow F_{Ay}\sqrt{l^2 - d^2} = M_j \quad \text{(Horizontal restraint released)} \tag{9}$$

where l_2 is the horizontal distance between F_{Ay} and F_{By}. In this model, no axial force develops in the beam. By treating the right term of the equation independently, Eq. (7) can be rewritten as follows:

$$F_{Ay}\sqrt{l^2 - d^2} = M_j \Rightarrow \frac{F_{Ay}\sqrt{l^2 - d^2}}{l} = \frac{M_j}{l} \Rightarrow \frac{F_{Ay}\sqrt{l^2 - d^2}}{l} = M_1 \quad \text{(Horizontal restraint released)} \tag{10}$$

F_{Ay} can be obtained by solving the detailed numerical models with their horizontal restraint released. Then, according to Eq. (8), M_1 can be derived. M_1 represents the flexural contribution without the influence of *M-N* interaction.

To gain a deeper understanding of the joint behaviour, detailed numerical models were developed to investigate the four joints as shown in Fig. 10. The numerical models include rigid joints (welded connection) and semi-rigid joints (bolted connection) with pinned ends at the beam extremities. Their connection details and modelling methods are the same as previously shown in Fig. 3. Considering the configuration of the parking structure (Fig. 2(c)), the representative beam length were taken as 2400 mm for the *x*-direction joints (RX-2400 and SX-2400) and 4800 mm for the *y*-direction joints (RY-4800 and SY-4800), respectively. "R(*S*)X-2400" represents the rigid (semi-rigid) joint in *x*-direction. In the reported results, "*P*" denotes the vertical load; "*M*" and "*C*" represent the contributions coming from the flexural action and catenary action as reflected in Eq. (6), respectively; "M_1" stands for the contribution from the flexural action without considering *M-N* interaction. Since the numerical models are symmetric, the vertical loads (shown as *y*-axial in Fig. 10) were taken as half to represent the contributions from one side of the joint.

Published in : Journal of Constructional Steel Research (2024), vol. 213, 108355
DOI: 10.1016/j.jcsr.2023.108355
Status : Postprint (Author's version)

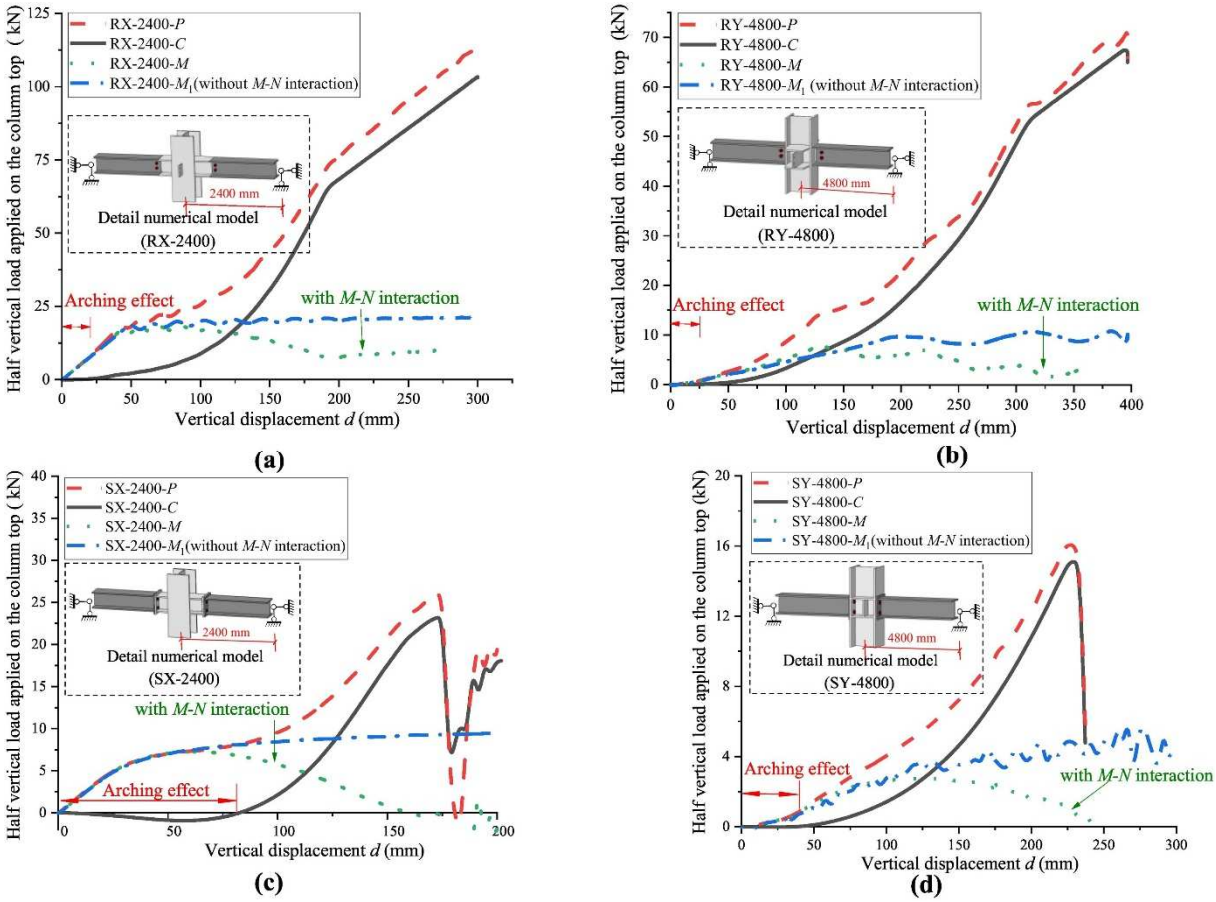

Fig. 10. Relationship between *P*, *C*, *M*, and M_1 for the detailed numerical models of the investigated joints: (a) RX-2400; (b) RY-4800; (c) SX-2400; (d) SY-4800.

The relationship between *P*, *C*, *M*, and M_1 of the different joints can be seen in Fig. 10. It can be observed that, for the cases of semi-rigid joints (SX-2400-C and SY-4800-C), a "negative" contribution from the catenary action for a rather small value of the vertical displacement of the system is obtained. This phenomenon is also observed in the rigid joints (RX-2400-C and RY-4800-C) but for smaller vertical displacements. The extent of this "negative" contribution of *C* represents the degree of influence of arching effect on the response of the system. So, from the investigated joints, it can be concluded that the arching effect is not significant in the case of rigid joints and so can be neglected.

Another observation is that, in all cases, the flexural action (*M*) provides a main contribution when the vertical displacement is small. But, when vertical displacement becomes significant, the catenary action (*C*) gradually increases and finally plays a dominant role in the overall capacity of the system. It should be noted that the flexural action (*M*) does not always increase or remain constant. Indeed, it can decrease due to the *M-N* interaction developing at the level of the joints. To clearly demonstrate the influence of this interaction, Fig. 10 also gives the curves of the flexural action without considering *M-N* interaction "M_1" (blue line in Fig. 10). The comparison between the green and blue lines shows a discrepancy at a large vertical displacement. For example, when the displacement reaches 250 mm, the discrepancy between the green and blue lines of RX-2400 is 55.1%, and for RY-4800 at 300 mm, it is 63.6%. It is noteworthy that for SX-2400 and SY-4800, the blue

Published in : Journal of Constructional Steel Research (2024), vol. 213, 108355
DOI: 10.1016/j.jcsr.2023.108355
Status : Postprint (Author's version)

line will decrease to zero at 158 mm and 147 mm, respectively. The above indicates that, if the traditional method is used to predict the joint response (without considering *M-N* interaction), the vertical loads supported by the system will be overestimated.

To address the limitation of the traditional method, an innovative method will be proposed in the subsequent section by focusing on the two key aspects, namely the arching effect and *M-N* interaction, to predict the robustness of joints in a more reasonable and convenient manner.

3.3. PROPOSED INNOVATIVE METHOD

3.3.1. ARCHING EFFECT

In the detailed numerical model developed with solid elements, the beam extremities were assumed to be pinned. When the system starts to deform (Fig. 11(a)), the beams are subjected to bending but also to compression forces as the extremities of the beams are horizontally fixed. When vertical displacements reach d_a (Fig. 11(b)), the arching effect is overcome and the axial force in the beam turns into tension.

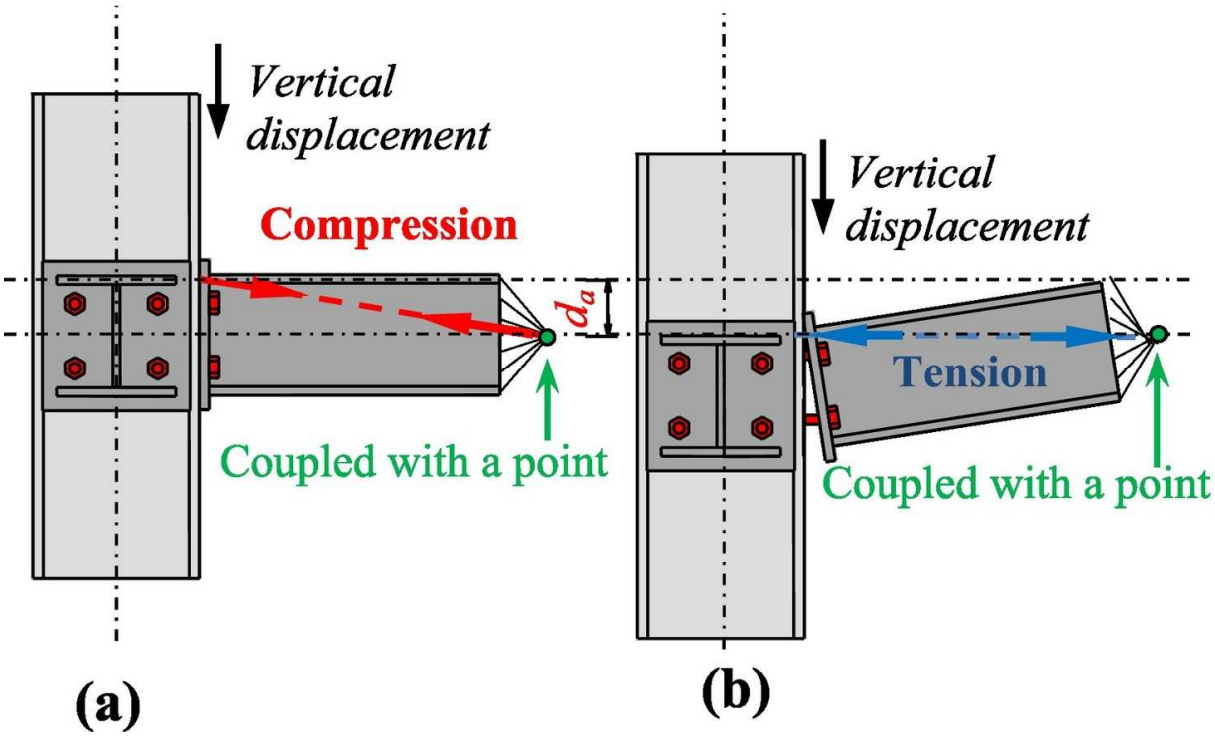

Fig. 11. Mechanism of the arching effects: (a) beam under compression; (b) beam under tension.

In fact, the determination of d_a is not straightforward because it is related not only to the beam height but also to the connections' detailing. As a simplification in the present work, it is assumed that d_a is equal to the distance from the flange centre to the section centre (corresponding to the vertical position of the pin-end), which can be expressed as follows:

$$d_a = \frac{h - t_f}{2} \quad (11)$$

Published in : Journal of Constructional Steel Research (2024), vol. 213, 108355
DOI: 10.1016/j.jcsr.2023.108355
Status : Postprint (Author's version)

where d_a represents the vertical displacement along which the arching effect is activated; h is the beam height; t_f is the thickness of the beam flange.

Typically, the conventional rotational springs provide only rotational restraint which cannot accurately account for the arching effect without a specific treatment [38]. In the current research work, the arching effect is accounted for in the model through the addition of a spring S_a as shown in Fig. 12 (a). The spring S_a (red spring) provides a negative stiffness in the range of $\Delta\delta_a$ (Fig. 12(b)). By combining S_h (black spring) and S_a (red spring), the arching-horizontal spring S_{ah} can be obtained (green spring). Since the arching-horizontal spring S_{ah} does not provide stiffness before S_{ah} reaches the displacement $\Delta\delta_a$, there is no axial force developing in the beam until the vertical displacement d_a is reached, as shown in Fig. 12(c). It is important to note that because the arching-horizontal spring S_{ah} is employed in this method, the compressive contribution of the arching effect is neglected, but its presence is conservatively accounted for by shifting the onset of the tensile stage. Therefore, in this approach, the compressive force resulting from the arching effect is assumed to be zero. It is acceptable since, for the specific structural system studied within the present paper, the compressive force is relatively small as demonstrated in Fig. 10.

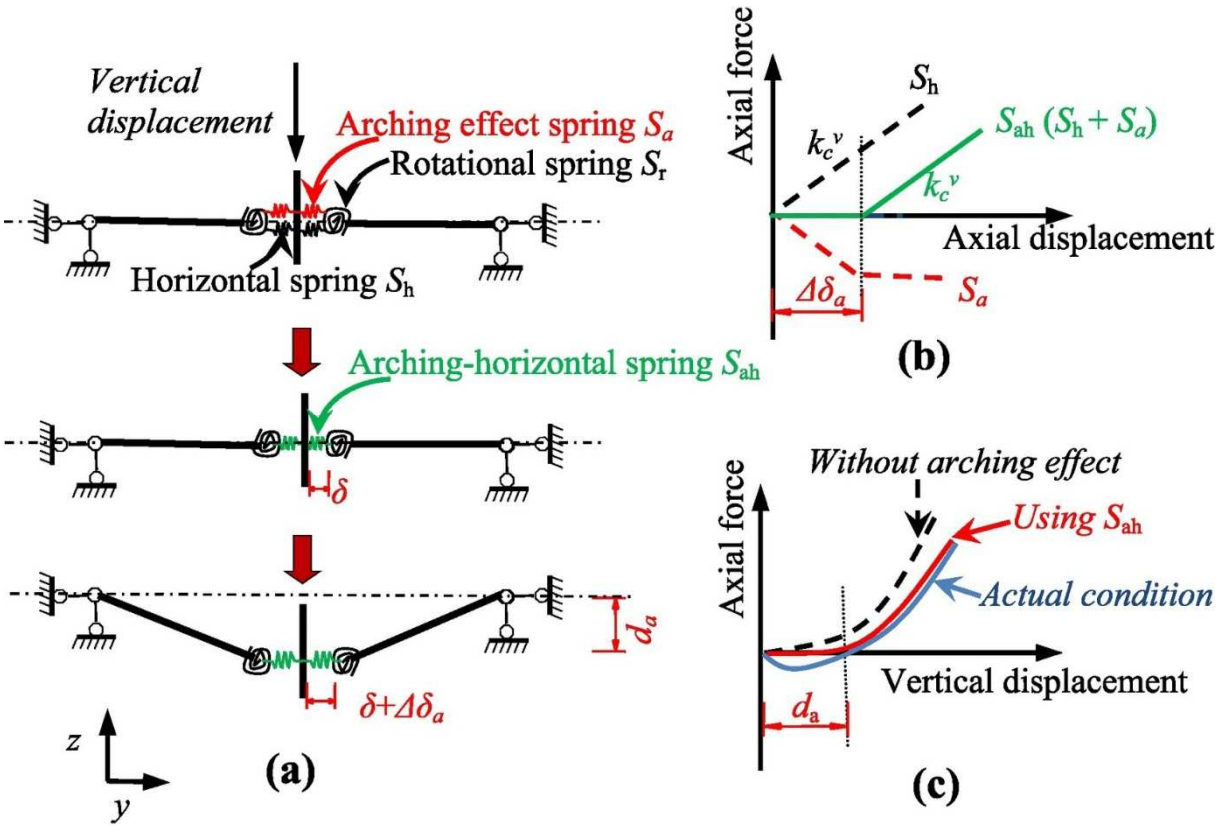

Fig. 12. (a) Development of mechanical models; (b) calculation on the stiffness of the arching-horizontal spring; (c) comparison of the axial force-vertical displacement curve of joints between the different conditions.

The relationship between the $\Delta\delta_a$ and d_a can be derived based on the geometry, and can be expressed as follows:

Published in : Journal of Constructional Steel Research (2024), vol. 213, 108355
DOI: 10.1016/j.jcsr.2023.108355
Status : Postprint (Author's version)

$$\Delta\delta_a = \frac{\left(\sqrt{d_a^2 + l^2} - l\right)EA}{lk_c^v} \quad (12)$$

where $\Delta\delta_a$ is the range of the distance considering a stiffness equal to zero in the arching effect spring S_a; A is the area of the beam cross-section; k_c^v is the axial stiffness of the connection. Based on Eq. (10), the calculated values of $\Delta\delta_a$ for the connections in the corresponding joints are presented in Table 3.

Table 3. Definitions of the arching-horizontal and rotational springs.

Connection types	**Investigated joints**	$\Delta\delta_a$	**A** (x_a, y_a)	**B** (x_b, y_b)	**C** (x_c, y_c)	**D** (x_d, y_d)
Welded connection-2400	RX-2400	/	(8.6, 1)	(57.3, 0.92)	(132.5, 0.01)	(250, 0.02)
Welded connection-4800	RY-4800	/	(10.1, 1)	(88.7, 1.06)	(255.2, 0.29)	(400, 0.45)
Bolted connection −2400	SX-2400	1.411	(15.4, 1)	(58.0, 1.35)	(124.2, 1)	(190, 0)
Bolted connection −4800	SY-4800	0.353	(31.2,1)	(80.1, 1.37)	(169.0, 1)	(260, 0)

Note: x_m and y_m (m = a, b, c, and d) is the coordinates on the curve $m(d)$ with an example shown in Fig. 14(a); "welded connection-2400" represents the welded connection with the length of the connected beam is 2400 mm.

3.3.2. MOMENT-AXIAL FORCE INTERACTION

The axial force has a significant effect on the global response of the joint. Therefore, the mechanical properties assigned to the rotational spring S_r must consider the influence of this axial force. For the welded connections, they can be characterised as full-strength joints and thus the plastic hinge occurs in the beam rather than the connection. As a consequence, the *M-N* interaction developing in the system will in fact develop at the level of the beam. This interaction has been previously studied by the authors [36], and can be expressed as follows:

Published in : Journal of Constructional Steel Research (2024), vol. 213, 108355
DOI: 10.1016/j.jcsr.2023.108355
Status : Postprint (Author's version)

$$m_r = \begin{cases} 1 - \dfrac{P_y^{\,2}}{4 f_y t_w M_{beam}} n_r^{\,2}, n_r \in \left(0, \dfrac{P_w}{P_y}\right) \\ 1 + \dfrac{hP_w}{4M_{beam}} - \dfrac{hP_y}{2M_{beam}} n_r, n_r \in \left[\dfrac{P_w}{P_y}, 1\right) \end{cases}, P_w = f_y h_w t_w \ \text{(welded connection)} \tag{13}$$

where m_r is the normalized bending moment; n_r is the normalized axial force; P_y is the beam's ultimate strength.

For the bolted connections, their strength is governed by the bolt rows resistance, and, as a safe assumption, the expression of the *M-N* interaction can be linearly expressed as follows:

$m_r = 1 - n_r$ (bolted connection) (14)

According to Eq. (11) and Eq. (12), the curves of *M-N* interaction can be depicted as illustrated in Fig. 13.

To obtain the modified moment (i.e., the moment taking into account the *M-N* interaction), it is necessary to know the axial force in the connection, which is related to the deformation of the structural system. Based on the geometry of the problem shown in Fig. 12(a), the relationship between the axial force and vertical displacement can be expressed as follows:

$$P_{axial}(d) = \begin{cases} 0 & , 0 \le d < d_a \\ \dfrac{\left(\sqrt{(d-d_a)^2 + l^2} - l\right) EA}{l} & , d_a \le d \end{cases} \tag{15}$$

where $P_{axial}(d)$ is the axial force in the beam neglecting the compressive force from the arching effect but considering its compressive stage.

Since the axial force in the beam remains limited until the connection reaches its plastic moment capacity [36], it is assumed that the bending moment of the joint is not affected by the axial force at the beginning of the column removal, i.e. for displacements $d < d_1$ (Fig. 14). It can be expressed as follows:

$$m(d) = \frac{M_c^{\theta}\left(\frac{d}{l}\right)}{M_{plastic}} \Rightarrow m(d) = m_c^{\theta}(d), d < d_1 \tag{16}$$

Published in : Journal of Constructional Steel Research (2024), vol. 213, 108355
DOI: 10.1016/j.jcsr.2023.108355
Status : Postprint (Author's version)

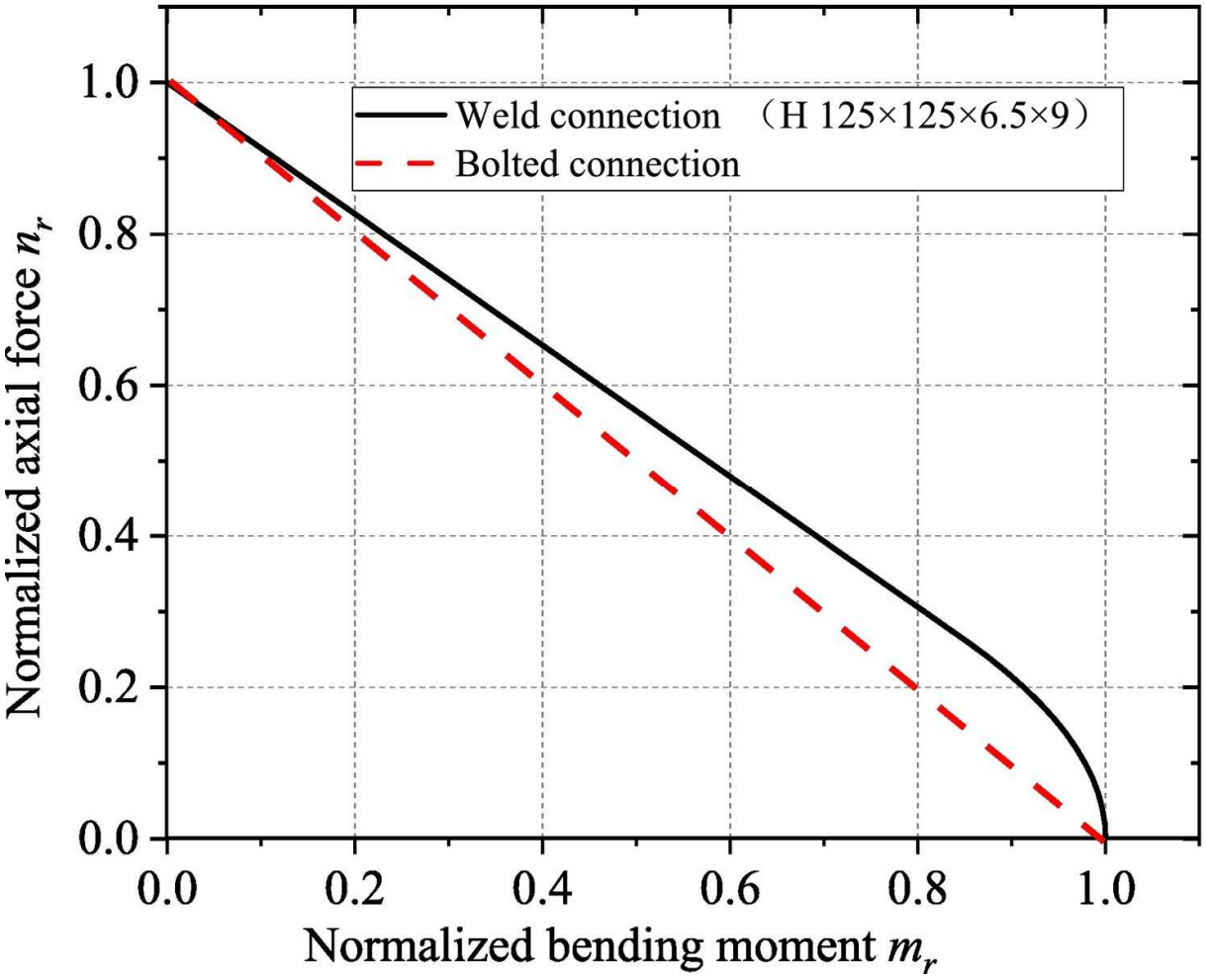

Fig. 13. Relationship of the *M-N* interactions.

where $m(d)$ is the modified normalized moment of the connection; $m_c^{\vartheta}(d)$ is the original normalized moment of the connection; d_1 represents the vertical displacement corresponding to the formation of the plastic mechanism in the system; $M_{plastic}$ is the original plastic moment capacity of the connection ($M_{plastic} = M_c^{\vartheta}(\vartheta_1)$) which is used to normalize the formula.

Published in : Journal of Constructional Steel Research (2024), vol. 213, 108355
DOI: 10.1016/j.jcsr.2023.108355
Status : Postprint (Author's version)

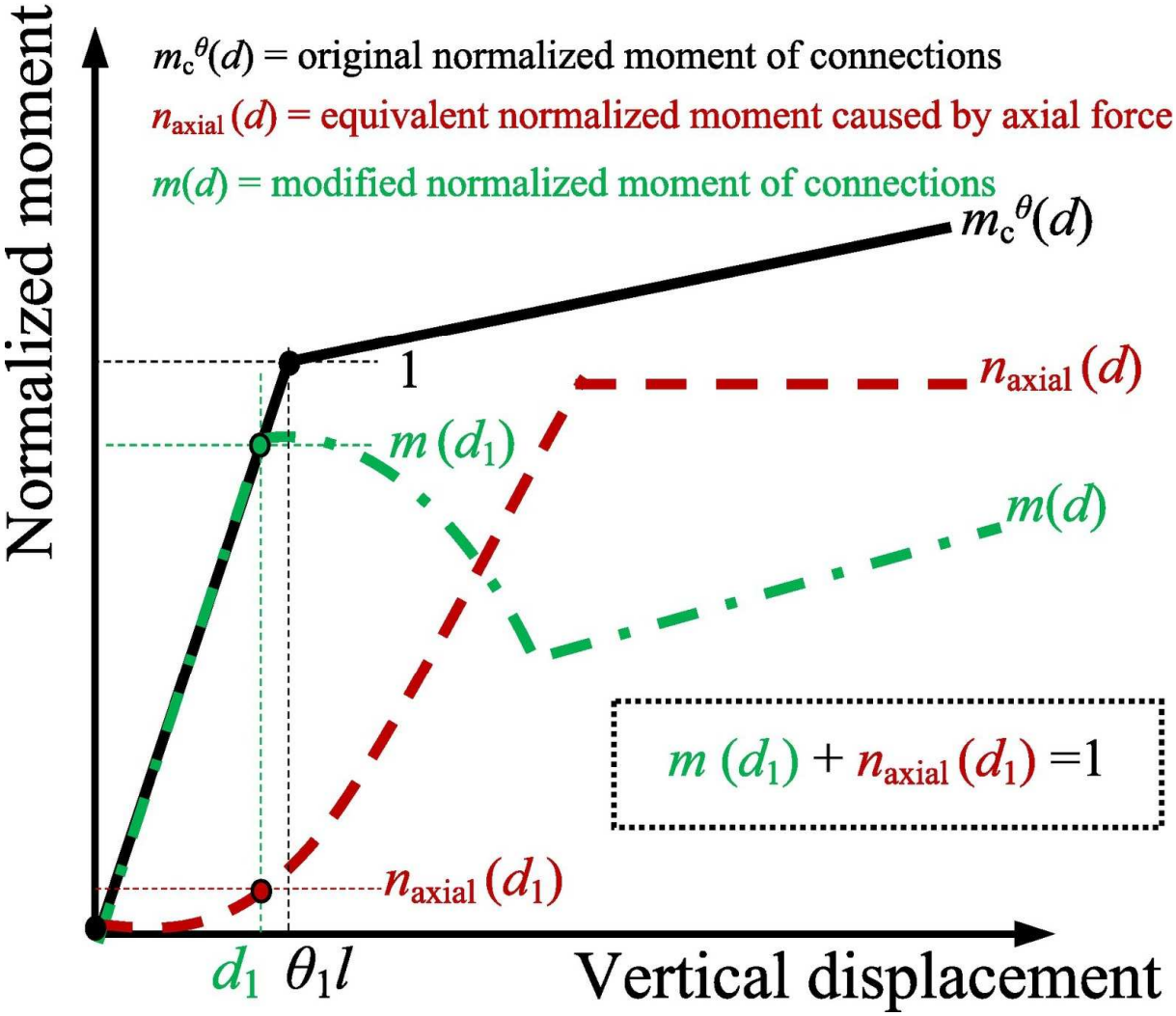

Fig. 14. Relationship of between the $m_c^{\vartheta}(d)$, $m(d)$, and $n_{axial}(d)$

When the joint reaches a displacement $d \geq d_1$, the connection enters the plastic stage, and the plastic moment capacity of the connection starts to decrease under the influence of the axial force. Under this situation, $m(d)$ can be expressed as follows:

$$m(d) = \frac{M_c^{\theta}\left(\frac{d}{l}\right)}{M_{plastic}} - n_{axial}(d) + n_{axial}(d_1) \Rightarrow m(d)$$
$$= m_c^{\theta}(d) - n_{axial}(d) + n_{axial}(d_1), d \geq d_1 \quad (17)$$

where $n_{axial}(d)$ is the equivalent normalized moment caused by axial force. Notably, the expression of $n_{axial}(d)$ is different in welded and bolted connections, according to Eqs. (13), (14). For the welded connection, by combining with Eq. (11), $n_{axial}(d)$ can be derived as follows:

Published in : Journal of Constructional Steel Research (2024), vol. 213, 108355
DOI: 10.1016/j.jcsr.2023.108355
Status : Postprint (Author's version)

$$n_{\text{axial}}(d)=\begin{cases}\dfrac{P_{\text{axial}}(d)^2}{4f_y t_w M_{\text{beam}}}, P_{\text{axial}}(d)\in(0,P_w) \\ \dfrac{hP_w}{4M_{\text{plastic}}}-\dfrac{hP_{\text{axial}}(d)}{2M_{\text{beam}}}, P_{\text{axial}}(d)\in[P_w,P_y)\end{cases} \quad \text{(welded connection)} \tag{18}$$

For the bolted connection, by combining Eq. (12), the expression of $n_{\text{axial}}(d)$ is as follows:

$$n_{\text{axial}}(d)=\frac{P_{\text{axial}}(d)}{P_y} \quad \text{(bolted connection)} \tag{19}$$

Substituting Eq. (16) and Eq. (17) into Eq. (14) and Eq. (15), respectively, the equations can be expressed as follows:

$$m(d)=\begin{cases}\dfrac{M_c^{\theta}(d/l)}{M_{\text{plastic}}} & ,d<d_1 \\ \dfrac{M_c^{\theta}(d/l)}{M_{\text{plastic}}}-\dfrac{{P_{\text{axial}}}^2(d)}{4f_y t_w M_{\text{plastic}}}+n_{\text{axial}}(d_1), P_{\text{axial}}(d)\in(0,P_w) & \text{(welded connection)} \\ \dfrac{M_c^{\theta}(d/l)}{M_{\text{plastic}}}-\dfrac{hP_w}{4M_{\text{plastic}}}+\dfrac{hP_{\text{axial}}(d)}{2M_{\text{plastic}}}+n_{\text{axial}}(d_1), \dfrac{P_{\text{axial}}(d)}{P_y}\in[P_w,P_y) & ,d\geq d_1\end{cases} \tag{20}$$

$$m(d)=\begin{cases}\dfrac{M_c^{\theta}(d)}{M_{\text{plastic}}} & ,d<d_1 \\ \dfrac{M_c^{\theta}(d)}{M_{\text{plastic}}}-\dfrac{P_{\text{axial}}(d)}{P_y}+n_{\text{axial}}(d_1) & ,d\geq d_1\end{cases} \quad \text{(bolted connection)} \tag{21}$$

Fig. 15 illustrates the calculation of $m(d)$ for the welded and bolted connections based on Eq. (18) and Eq. (19), respectively, wherein "welded connection-2400" and "welded connection-4800" are used in the joints "RX-2400" and "RY-4800"; "bolted connection-2400" and "bolted connection-4800" are corresponding to the joints "SX-2400" and "SY-4800", respectively. The curves of $m(d)$ can be represented by a four-segment line (OA-AB-BC-CD). Examples of such lines are shown in Figs. 15(a) and 15(c), with the corresponding data listed in Table 3.

Published in : Journal of Constructional Steel Research (2024), vol. 213, 108355
DOI: 10.1016/j.jcsr.2023.108355
Status : Postprint (Author's version)

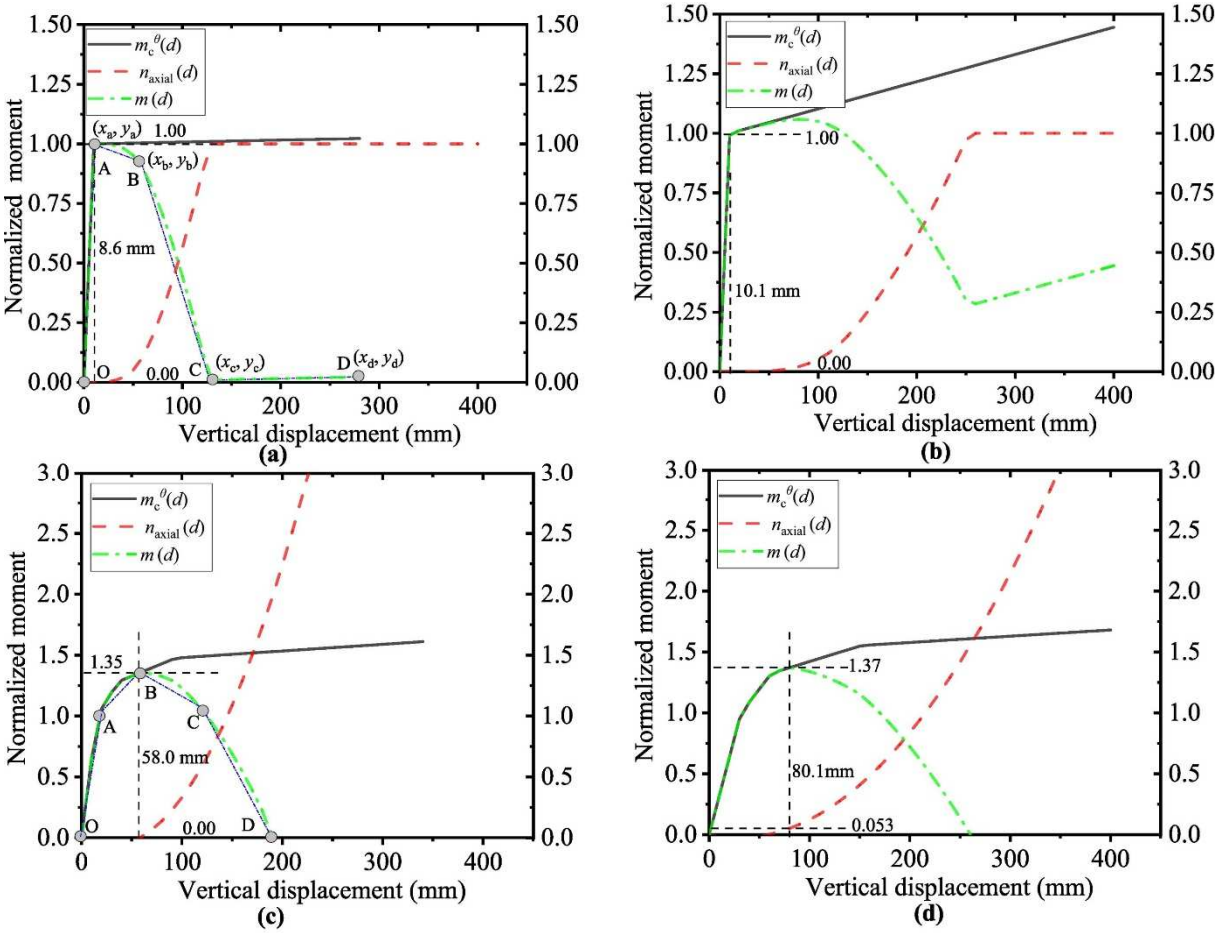

Fig. 15. Calculation of $m(d)$ for the different connections: (a) welded connection-2400; (b) welded connection-4800; (c) bolted connection-2400; (d) bolted connection-4800.

It is important to note that the innovative simplified method has some limitations due to the adopted assumptions and simplifications: (1) the actual characteristics of the connection need to be obtained before using the method, as illustrated in Section 2.4; (2) the method is only applicable to simple and typical connections commonly found in parking structures, and may not perform well for more sophisticated connections with strong coupling effects between their rotational and axial stiffness.

3.3.3. MECHANICAL CHARACTERIZATION OF THE STUDIED CONNECTIONS

The incorporation of the arching effect and *M-N* interaction has been addressed above. On this basis, a simplified numerical mechanical model has been developed in Abaqus/Explicit in which the column and beam are modelled by beam elements (type B31) as illustrated in Fig. 16(a). Between the beam and the column, rotational and arching-horizontal springs were set to represent the mechanical characteristics of the investigated connections (Fig. 16(b)). Unlike the traditional method which does not account for the arching effect, the arching-horizontal spring S_{ah} includes a zero stiffness range ($\Delta\delta_a$) in the bolted connection to address this issue, as referred to in Section 3.3.1. On the other hand, the rotational spring S_r incorporates the *M-N* interaction, as discussed in Section 3.3.2. The corresponding data used for defining the springs are reported in Table 3.

Published in : Journal of Constructional Steel Research (2024), vol. 213, 108355
DOI: 10.1016/j.jcsr.2023.108355
Status : Postprint (Author's version)

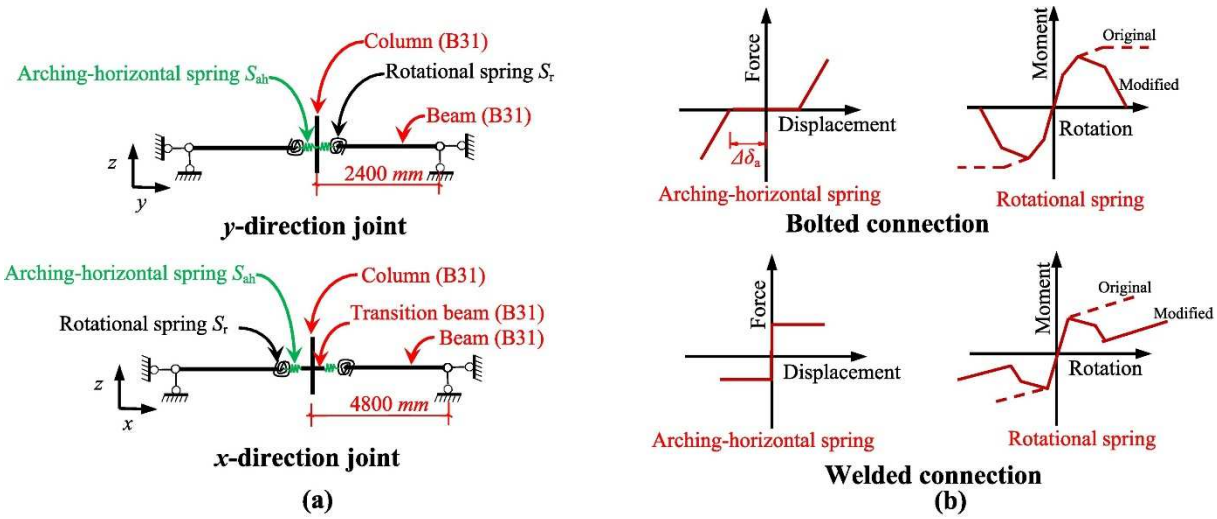

Fig. 16. Definition of the springs in simplified numerical models: (a) simplified numerical models; (b) stiffness characteristics of the springs.

3.4. VALIDATION OF THE INNOVATIVE METHOD

Fig. 17 shows the comparisons of the numerical results between the detailed and proposed simplified models. The compared models include two types of boundary conditions: with and without horizontal restraints at the beam extremities. In cases of semi-rigid joints (Figs. 17(c) and 17(d)), a relatively large discrepancy in the results between the simplified and detailed models is observed at the end of the curve, i.e. for large deformation. This is because the rotational and arching-horizontal springs in the simplified models do not incorporate the material degradation and fracture, which leads to a slight overestimation of the system's resistance. Apart from this, all the results from the simplified model are in good agreement with the ones from the detailed models, which validate the use of the proposed model. In the subsequent section, this method for joint modelling will be implemented in the analyses of global parking structures.

Published in : Journal of Constructional Steel Research (2024), vol. 213, 108355
DOI: 10.1016/j.jcsr.2023.108355
Status : Postprint (Author's version)

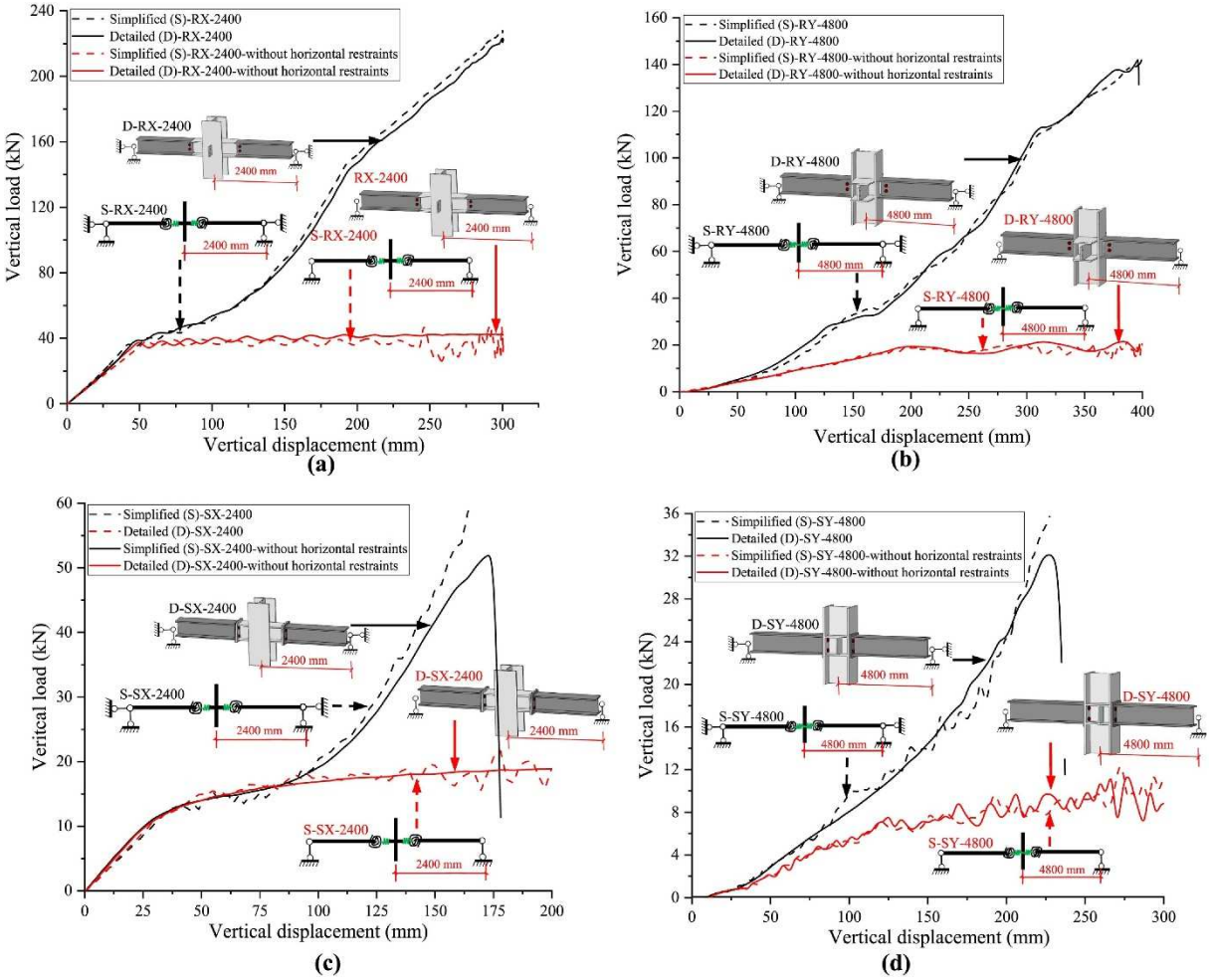

Fig. 17. Comparisons of the joint vertical load against displacement curve between the simplified (S) and detailed (D) numerical models: (a) RX-2400; (b) RY-4800; (c) SX-2400; (d) SY-4800.

4. Implementation of the innovative method in structural analyses

4.1. ADOPTED METHODOLOGY

To clearly illustrate the proposed method, Fig. 18 provides a flow chart of the methodology. The flow chart can be divided into three parts: the design, the definition of the springs (rotational springs and arching-horizontal springs), and the development of the sub-structure model. (1) In the design, the detailing of the connection is fixed and the main properties of the typical joint are computed. (2) The connection stiffness cannot be directly obtained; thus it is necessary to extract the connection stiffness from the typical joint stiffness. After that, the behaviour law of the connection is modified by considering the influence of arching effect and *M-N* interaction. Finally, the modified behaviour law is implemented in the substructure model through rotational and arching-horizontal springs. The method to extract the substructure model from the global structure is discussed in the following

Published in : Journal of Constructional Steel Research (2024), vol. 213, 108355
DOI: 10.1016/j.jcsr.2023.108355
Status : Postprint (Author's version)

section where the definition of the springs at the boundaries of the substructure through the analysis of the overall structure is explained. Finally, the behaviour of parking structures subjected to a column loss scenario is predicted using the sub-structure model and compared to the global structure analysis response.

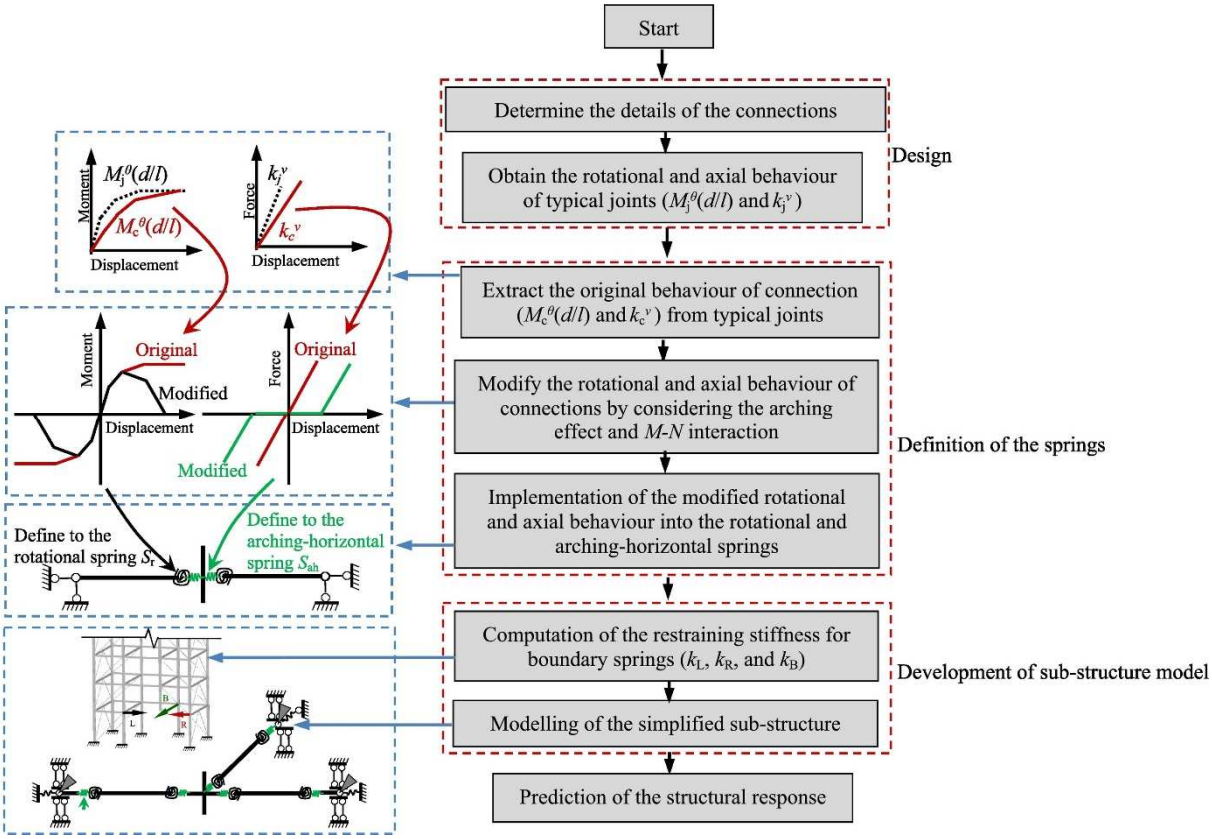

Fig. 18. Flow chart of the procedure on predicting the behaviour of parking-structure joints.

4.2. DEVELOPMENT OF A SUB-STRUCTURE MODEL

Fig. 19 shows a global model of the parking structure whose configuration is the same as the structure previously shown in Fig. 2(b). Previously, Izzuddin et al. [18] provided an approach to simplify a global model into a sub-structure model. Following their method, a similar sub-structure is exhibited, extracted from the global structure as marked with a red line in Fig. 19(a), and is modelled as shown in Fig. 20(a). At the beam extremities, the rotation and vertical displacement are blocked, while the horizontal displacement is restricted through springs simulating the boundary conditions provided by the rest of the structure. Since the horizontal displacement at the beam extremities will remain very small, the boundary springs are assumed to be linear elastic.

Published in : Journal of Constructional Steel Research (2024), vol. 213, 108355
DOI: 10.1016/j.jcsr.2023.108355
Status : Postprint (Author's version)

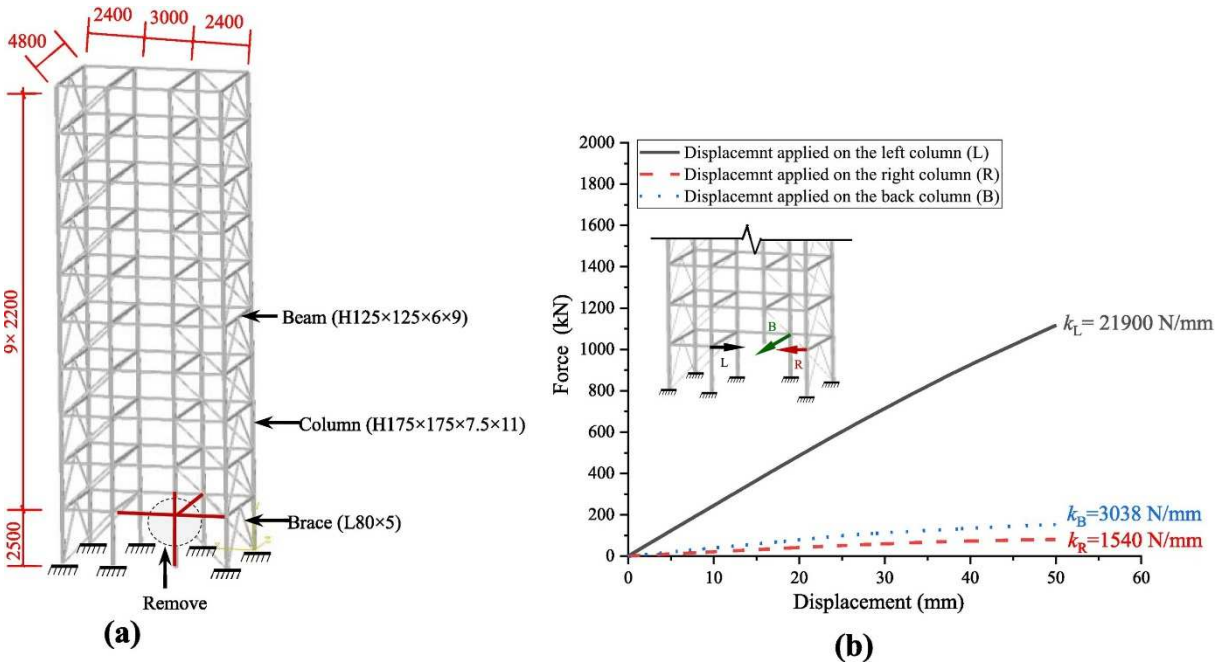

Fig. 19. Analyses of the steel parking structure: (a) global models; (b) boundary stiffness of the sub-structure model (in mm).

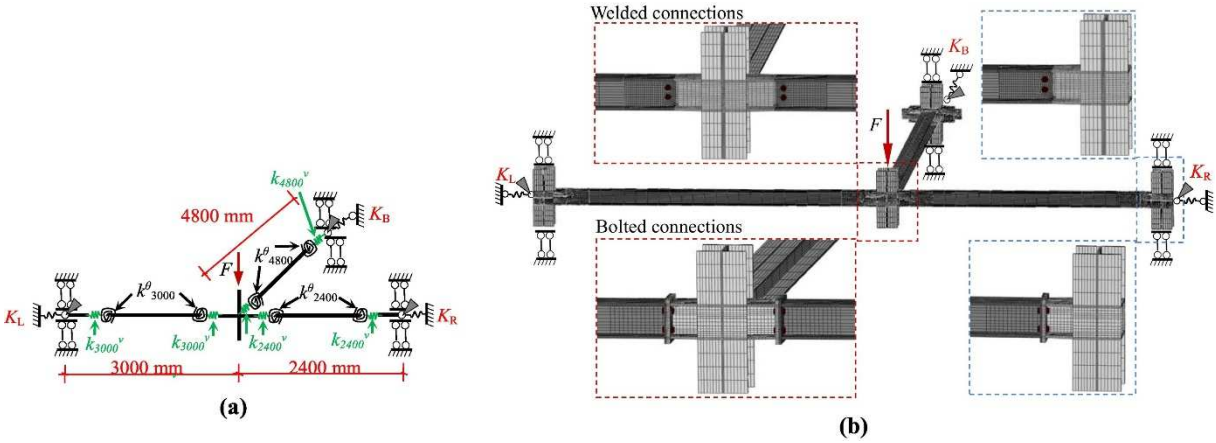

Fig. 20. Numerical models: (a) simplified sub-structure model and (b) detailed sub-structure model.

To obtain the restraining stiffness, a FE model of the global structure is built removing the sub-structure part; then, the so-defined remaining structure is subjected to loads in different directions separately, as shown in Fig. 19(b), to derive the restraining stiffness at the level of the left beam (k_L), right beam (k_R), and back beam (k_B). It should be noted that, for simplification, the beam-column connections in the remaining structure are treated as rigid. The boundary stiffness of the sub-structure can be calculated as follows:

$$K_R = K_L = \frac{k_R k_B}{k_B + k_R} \quad (22)$$

$$K_B = 0 \quad (23)$$

where K_R,K_L and K_B are the boundary stiffness of the sub-structure at the right, left and back beam extremities, respectively.

Published in : Journal of Constructional Steel Research (2024), vol. 213, 108355
DOI: 10.1016/j.jcsr.2023.108355
Status : Postprint (Author's version)

The axial force developing in the beams is affected by the beam boundary condition. Accordingly, the behaviour laws of the rotational spring simulating the connections need to be recalculated using the same approach as presented in Section 3.3.2. The curves reflecting the behaviour of the welded and bolted connections (k^{ϑ}_{3000}, k^{ϑ}_{2400}, and k^{ϑ}_{4800}) are presented in Fig. 21. Regarding the arching-horizontal springs, the axial stiffness of the *x*-direction (k_{2400} and k_{3000}) and *y*-direction (k_{4800}) bolted connections are taken as 11,280 and 10,840 N/mm, respectively, as presented in Table 2.

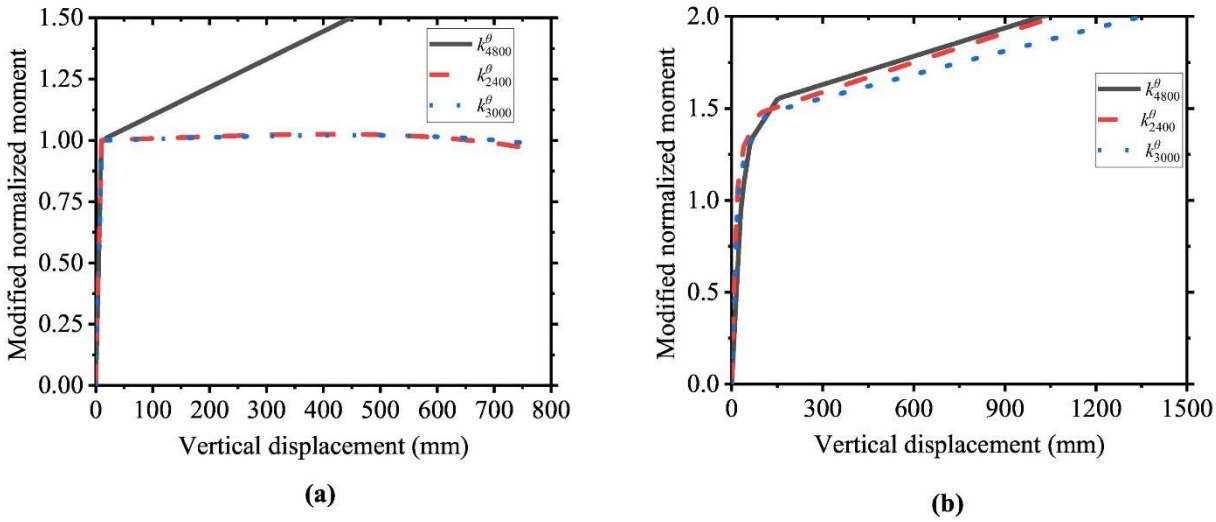

Fig. 21. Curves of the vertical displacement against modified normalized moment for the different connections in parking structures: (a) welded connections; (b) bolted connections.

Instead of performing an analysis under displacement control, a force is applied on the sub-structure to simulate the column loss. In the previous research [39], the duration of the scenario that a vehicle impacts the column ranges from 0.06 s to 0.1 s which is correlated with the impact velocities. Consequently, the period of the loading from zero to maximum is taken as 0.1 s in these cases. On the other hand, according to [40], the load capacity of the column *N* and the equivalent vertical load on the joint *F* can be expressed as follows:

$\varphi A_c f_y = N$ (24)

$$F = \frac{N}{n_s} \quad (25)$$

where *N* is the load capacity of the column; *F* is the equivalent vertical load on the joints; φ is the stability coefficient of axially compressive members, which is taken as 0.728 [39]; A_c is the area of the column section; n_s is the number of the structural storeys (here fixed at 10). Based on Eqs. (24), (25), *F* is estimated as equal to 105.2kN.

4.3. VALIDATION OF THE PROPOSED METHODOLOGY

To validate the proposed methodology, detailed sub-structure models are numerically built and compared with the simplified sub-structure models in terms of overall response. Fig. 20(b) shows the two detailed models with welded and bolted connections, respectively. Both are modelled with solid elements (C3D8R) as described and previously validated in Section 2.4. The used materials, the

Published in : Journal of Constructional Steel Research (2024), vol. 213, 108355
DOI: 10.1016/j.jcsr.2023.108355
Status : Postprint (Author's version)

boundary conditions and the applied loading are the same for both detailed and simplified models. Fig. 22 shows the comparisons of the joint response predicted by the two different models. A very good agreement between the results provided by the two models is observed, thus validating the proposed simplified model. This method exhibits several advantages. The development of the simplified model is easier than the detailed model. For instance, for the model with welded connections, only 278 finite elements are used, which is tremendously less than the corresponding detailed model which includes 49,175 finite elements. Consequently, it requires less computational time: 13.4 s for the simplified model to be compared to 6848 s for the detailed model (performed on a computer with Intel(R) Core(TM) i7-12700H 2.70 GHz). This highlights the model's added value in terms of computational efficiency. In view of this, the proposed model can be used for a preliminary design in various scenarios such as in structures with damaged columns leading to joint failure, or for a quick estimation of the joint vertical displacement in collision events. The following section will demonstrate the model's application in different impact scenarios.

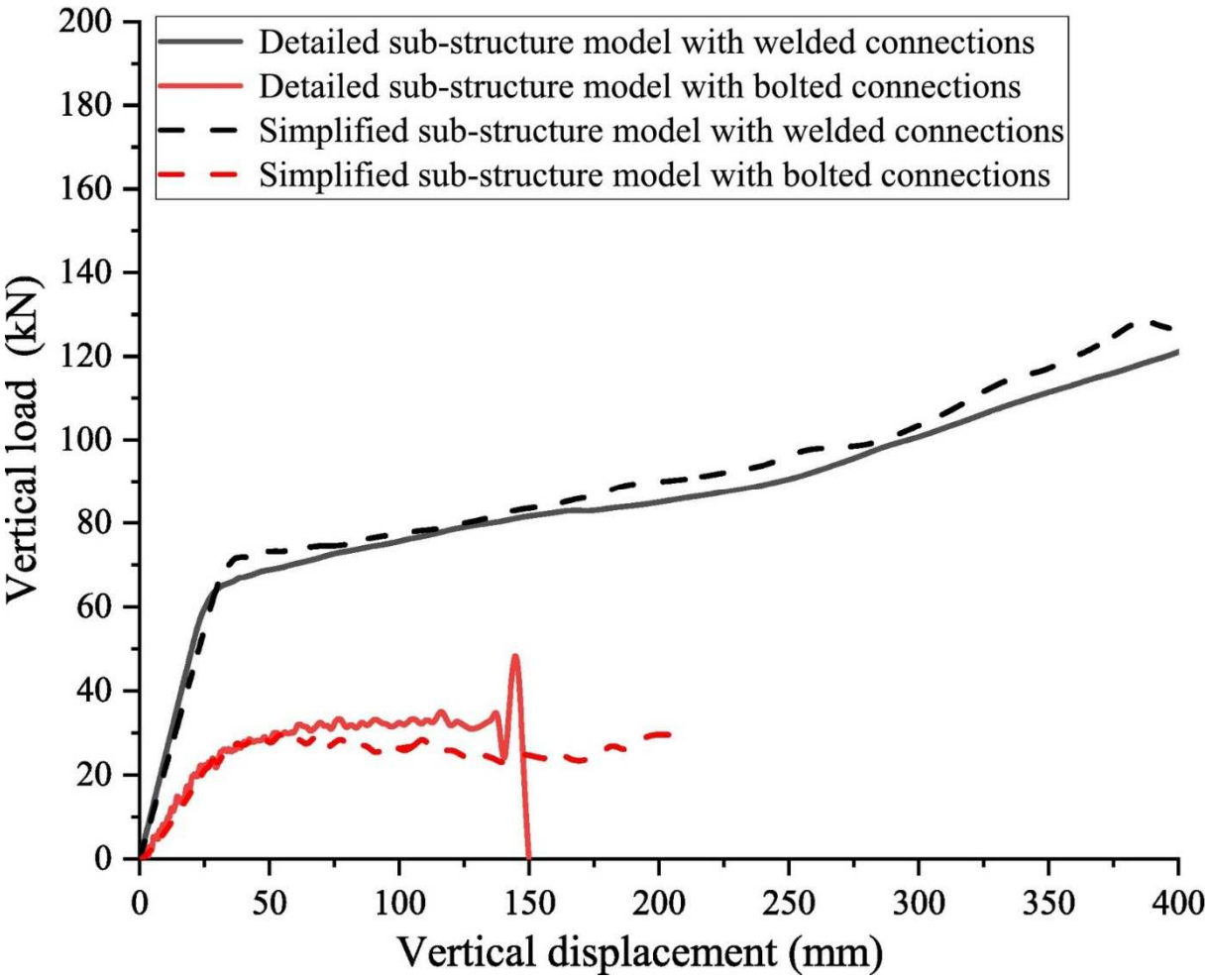

Fig. 22. Comparison of the vertical load against displacement curves between the detailed and simplified sub-structure models with welded and bolted connections.

Published in : Journal of Constructional Steel Research (2024), vol. 213, 108355
DOI: 10.1016/j.jcsr.2023.108355
Status : Postprint (Author's version)

5. Use of simplified sub-structure models for different impact scenarios on the reference structure

5.1. CONSIDERED IMPACT SCENARIOS

As previously shown in Fig. 2(c), the failure of joints is generally caused by the collision between the vehicles and columns. In most cases, the collision will lead to the reduction of the column's load-carrying capacity. This implies that the loads to be resisted by the beam-to-column joints increase. Additional vertical loads will be applied to the joints during the collision. Therefore, establishing a correlation between the impact scenarios and vertical loads, and then predicting the joint robustness can provide a more reasonable representation of the real situation. The purpose of this section is to demonstrate the usage scenarios of the proposed method and provide the corresponding design recommendations, thus offering references for engineers and designers. Xiang et al. [39] have conducted a study on the performance of the parking structure subjected to a frontal vehicular collision, with a focus on the column. Overall, the configuration of the previous parking structure is the same as the one investigated in the current research. In their study, a reduced vehicular model for a Chevrolet C1500 Pickup was used to impact the parking-structure column at velocities ranging from 10 km/h to 80 km/h. This type of vehicle was selected for analysis because it has undergone comprehensive validation previously, and its moderate mass and stiffness enable it to serve as a representative of common vehicles. Moreover, the utilization of the reduced vehicular model to represent the vehicle can reduce the modelling effort and computational cost. The mass-elastoplastic spring was employed to represent the vehicular stiffness during the collision, allowing the system to reflect the energy absorption of vehicles. Fig. 23 shows the results from their study, where the ratio of residual load-carrying capacities N_{res} to ultimate capacities N_u represents the damage degree of the column. As impact velocity increases, column damage becomes more severe, and the joint bears more loads. To prevent the collapse, it is important to identify the ultimate impact velocity inducing the failure of the joints. In this regard, compared to detailed numerical models, the proposed model (simplified sub-structure model, shown in Fig. 20(a)) manifests its advantages as the response of the structure can be easily and quickly predicted for different collision scenarios as reflected in the next section.

Published in : Journal of Constructional Steel Research (2024), vol. 213, 108355
DOI: 10.1016/j.jcsr.2023.108355
Status : Postprint (Author's version)

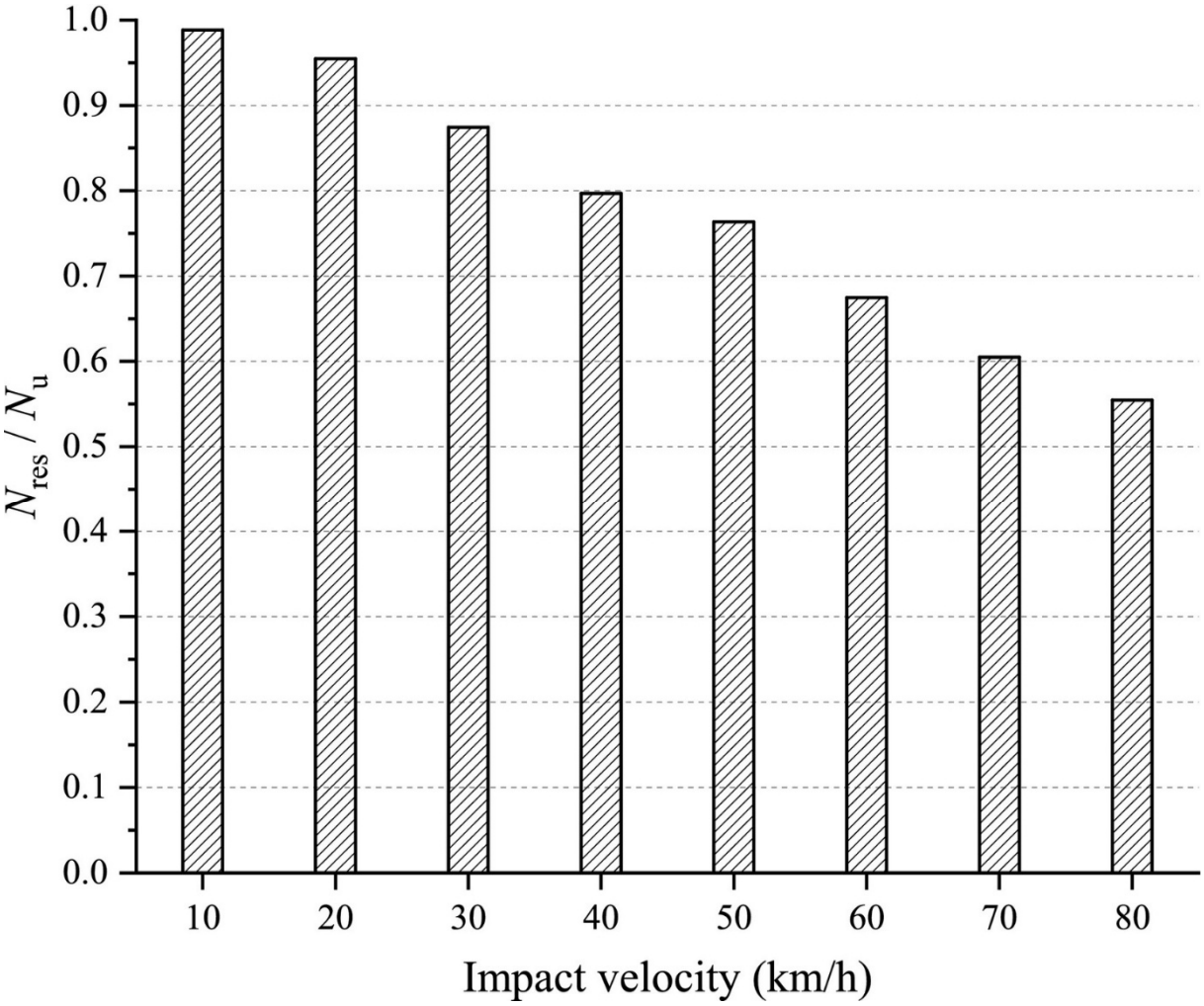

Fig. 23. Loss of the load capacity for columns subjected to vehicular collisions with different impact velocities [39].

5.2. ANALYSIS OF THE RESULTS

Fig. 24 shows the response of the sub-structure with welded and bolted connections under column collision with different impact velocities. It should be mentioned that, as recommended in [41], 20 km/h and 50 km/h are the key velocities which correspond to the car driving on the courtyard and urban roads respectively where the parking structure is typically located. It can be seen from the results that the welded connections lead to an enhanced structural robustness when compared to the response of sub-systems with bolted connections. The use of welded connections can effectively prevent the collapse of the parking structure subjected to normal impact velocities, regardless of its location. If bolted connections are adopted, the collapse will easily be triggered in the structure located near urban roads. Nonetheless, according to [42], vertical displacement should be limited to 10 mm to meet the parking function requirement. Based on this criterion, it can be concluded that, if the structure is built in the courtyard, both types of connections are suitable. When structures are built near urban roads, it may be necessary to adopt not only welded connections but also additional strategies to enhance the robustness of the joints in collision events. The determination

Published in : Journal of Constructional Steel Research (2024), vol. 213, 108355
DOI: 10.1016/j.jcsr.2023.108355
Status : Postprint (Author's version)

of a suitable joint typically involves significant computational cost, making the proposed method an attractive option for designers due to its simplicity and potential to save design time.

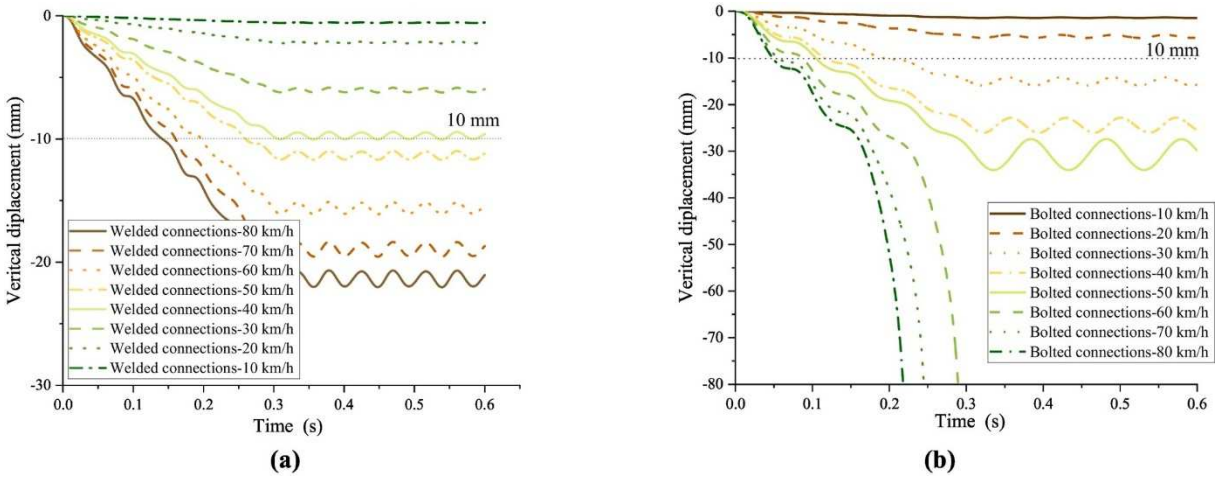

Fig. 24. Response under different impact velocities of the sub-structures with: (a) the welded and (b) bolted connections.

6. Conclusions

This study proposes an innovative and specific simplified method for incorporating the beam-to-column joint behaviour in the robustness assessment of steel parking structures. The proposed method addresses the issue of systematically disregarding the arching effect and *M-N* interaction in the conventional models with connections simulated through rotational springs. The proposed method relies on the definition of a simplified sub-structure model validated against the results from advanced numerical analyses. Given the accurate results and reduced computational cost, the proposed model was used to analyse the robustness of the steel parking structure under various impact scenarios with account for the joint behaviour. The main contributions and conclusions of this study are presented below.

(1) An approach for separating the connection stiffness from the joint stiffness is proposed. The approach allows for realistic characterization of typical connections in the steel parking structure.

(2) An innovative simplified method was proposed, enabling a conventional model to reflect the arching effect and the *M-N* interaction. This is achieved by defining two special springs, an arching-horizontal spring with a range of zero stiffness reflecting an arching effect by neglecting the compressive contribution but considering the compressive stage; and a rotational spring that captures the *M-N* interaction by coupling the vertical displacement with the connection moment capacity.

(3) A simplified sub-structure model incorporating the behaviour of connections was developed based on the proposed method allowing for the prediction of the collapse-resistance of the parking structure. In the particular case of the sub-structures with welded connections, the results show that

Published in : Journal of Constructional Steel Research (2024), vol. 213, 108355
DOI: 10.1016/j.jcsr.2023.108355
Status : Postprint (Author's version)

the simplified model can reduce the number of elements and computational time by 176 and 511 times, respectively, when compared to the detailed (advanced numerical) model.

(4) Examples of using the simplified sub-structure model for different impact scenarios were provided. It is recommended to adopt the bolted connection for structures built in the courtyard. However, if the structure is built near an urban road, welded connections with additional reinforcing strategies should be considered to enhance the structural robustness.

CRediT authorship contribution statement

Siyu Xiang: Conceptualization, Methodology, Software, Formal analysis, Writing – original draft. **Yongjun He:** Supervision, Funding acquisition. **Tudor Golea:** Methodology, Writing – review & editing. **Vincent Denoël:** Supervision, Writing – review & editing. **Jean-François Demonceau:** Supervision, Conceptualization, Writing – review & editing, Project administration.

Declaration of Competing Interest

We declare that we have no conflict of interest.

Acknowledgement

This work was financially supported by the China Scholarship Council (Grant no 202206130040) and the National Natural Science Foundation of China (Grant no 51890902), which are gratefully acknowledged.

Data availability

Data will be made available on request.

References

[1] Z. Li, L. Miao, Automated stereo-garage with multiple cache parking spaces—structure, system and scheduling performance, Autom. Constr. 119 (2020), 103377.

[2] C.C. Segura, L. Hamra, M. D'Antimo, et al., Determination of loading scenarios on buildings due to column damage, Structures. 12 (2017) 1–12.

Published in : Journal of Constructional Steel Research (2024), vol. 213, 108355
DOI: 10.1016/j.jcsr.2023.108355
Status : Postprint (Author's version)

[3] J.-F. Demonceau, L. Comeliau, V.L. Hoang, et al., How can a steel structure survive to impact loading? Numerical and analytical investigations, Open Civ. Eng. J. (2017) 11.

[4] K. Ke, Y. Chen, X. Zhou, et al., Experimental and numerical study of a brace-type hybrid damper with steel slit plates enhanced by friction mechanism, Thin-Walled Struct. 182 (2023), 110249.

[5] X. Zhou, Y. Huang, K. Ke, et al., Large-size shape memory alloy plates subjected to cyclic tension: towards novel self-centring connections in steel frames, Thin-Walled Struct. 185 (2023), 110591.

[6] H. Wang, J. Huo, M. Elchalakani, et al., Dynamic performance of retrofitted steel beam-column connections subjected to impact loadings, J. Constr. Steel Res. 183 (2021), 106732.

[7] D. Kukla, A. Kozlowski, Parametric study of steel flush and extended end-plate joints under column loss scenario, Eng. Struct. 237 (2021), 112204.

[8] M. Alrubaidi, H. Elsanadedy, H. Abbas, et al., Investigation of different steel intermediate moment frame connections under column-loss scenario, Thin-Walled Struct. 154 (2020), 106875.

[9] F. Dinu, I. Marginean, D. Dubina, Experimental testing and numerical modelling of steel moment-frame connections under column loss, Eng. Struct. 151 (2017) 861–878.

[10] M. Xu, S. Gao, L. Guo, et al., Study on collapse mechanism of steel frame with CFST-columns under column-removal scenario, J. Constr. Steel Res. 141 (2018) 275–286.

[11] H. Wang, J. Huo, Y. Liu, et al., Dynamic performance of composite beam-column connections subjected to impact loadings, J. Constr. Steel Res. 178 (2021), 106498.

[12] J.P. Jaspart, K W., Design of Joints in Steel and Composite Structures, Ernst & Sohn, a Wiley branch, Brussels, Belgium, 2016.

[13] BS EN 1993-1-1: 2006, Eurocode 3: Design of Steel Structures — Part 1–1: General Rules and Rules for Buildings, European Committee for Standardization, Brussels, Belgium, 2006.

[14] B. Meng, F. Li, W. Zhong, et al., Strengthening strategies against the progressive collapse of steel frames with extended end-plate connections, Eng. Struct. 274 (2023), 115154.

[15] L. Zheng, W.-D. Wang, Multi-scale numerical simulation analysis of CFST columncomposite beam frame under a column-loss scenario, J. Constr. Steel Res. 190 (2022), 107151.

[16] Y. Song, M.C. Yam, J. Wang, Enhanced progressive collapse resistance of bolted beam-to-column connections with ductile stainless steel components, Eng. Struct. 275 (2023), 115337.

[17] Advanced Steel Construction, F. Wang, J. Yang, Z. Pan, Progressive collapse behaviour of steel framed substructures with various beam-column connections, Eng. Fail. Anal. 109 (2020), 104399.

[18] B. Izzuddin, A. Vlassis, A. Elghazouli, et al., Progressive collapse of multi-storey buildings due to sudden column loss—part I: simplified assessment framework, Eng. Struct. 30 (2008) 1308–1318.

[19] A. Vlassis, B. Izzuddin, A. Elghazouli, et al., Progressive collapse of multi-storey buildings due to sudden column loss—part II: application, Eng. Struct. 30 (2008) 1424–1438.

Published in : Journal of Constructional Steel Research (2024), vol. 213, 108355
DOI: 10.1016/j.jcsr.2023.108355
Status : Postprint (Author's version)

[20] M. Geuzaine, J.-P. Jaspart, J.-F. Demonceau, et al., Influence of a small flexibility of connections on the elastic structural response of frames, J. Struct. Eng. 148 (2022) 04022033.

[21] T. Golea, J.-P. Jaspart, J.-F. Demonceau, Characterisation of the behaviour of beam-to-column steel joints up to failure, Adv. Steel Constr. 18 (2022) 679–686.

[22] T. Golea, A. Corman, J. Mathieu, et al., An innovative mechanical model for structural steel joints, Eng. Struct. 277 (2023), 115459.

[23] H. Zhang, X. Zhou, K. Ke, et al., Hybrid self-centering connection employing energy dissipation sequences: experimental study and a structural seismic demand perspective, J. Struct. Eng. 149 (2023) 04023157.

[24] H. Zhang, X. Zhou, K. Ke, et al., Self-centring hybrid-steel-frames employing energy dissipation sequences: insights and inelastic seismic demand model, J. Build. Eng. 63 (2023), 105451.

[25] B. Meng, W. Zhong, J. Hao, et al., Calculation of the resistance of an unequal span steel substructure against progressive collapse based on the component method, Eng. Struct. 182 (2019) 13–28.

[26] M. D'Antimo, M. Latour, G. Rizzano, et al., Experimental and numerical assessment of steel beams under impact loadings, J. Constr. Steel Res. 158 (2019) 230–247.

[27] S. Yan, K.J. Rasmussen, Generalised component method-based finite element analysis of steel frames, J. Constr. Steel Res. 187 (2021), 106949.

[28] Y. He, S. Xiang, X. Zhou, A reinforcing protection for steel parking-structure column under vehicular impact and design method, Thin-Walled Struct. 183 (2023), 110368.

[29] S. Xiang, Y. He, X. Zhou, et al., Continuous twice-impact analysis of steel parking structure columns, J. Constr. Steel Res. 187 (2021), 106989.

[30] SIMULIA, Abaqus Analysis user's Manual ver 6.14, vols. 3 and 5, Dassault Systèmes, Providence, Rhode Island, 2014.

[31] S. Xiang, Y. He, X. Zhou, Behaviour and failure modes of steel parking structure column under transverse impact, Thin-Walled Struct. 167 (2021), 108163.

[32] Y. Bao, T. Wierzbicki, On fracture locus in the equivalent strain and stress triaxiality space, Int. J. Mech. Sci. 46 (2004) 81–98.

[33] S. Yan, X. Zhao, A fracture criterion for fracture simulation of ductile metals based on micro-mechanisms, Theor. Appl. Fract. Mech. 95 (2018) 127–142.

[34] D. Li, B. Uy, J. Wang, et al., Behaviour and design of grade 10.9 high-strength bolts under combined actions. Steel, Compos. Struct. 35 (2020) 327–341.

[35] K. Damian, S. Tomasz, Numerical analysis of steel double side joints with flush and extended end plate under accidental situation, Ce/papers. 4 (2021) 77–84.

Published in : Journal of Constructional Steel Research (2024), vol. 213, 108355
DOI: 10.1016/j.jcsr.2023.108355
Status : Postprint (Author's version)

[36] S. Xiang, Y. He, X. Zhou, Simplified analytical procedure to calculate the impact behaviour of steel parking-structure columns, Structures. 46 (2022) 1938–1954.

[37] L. Duan, W.-F. Chen, A yield surface equation for doubly symmetrical sections, Eng. Struct. 12 (1990) 114–119.

[38] J.-F. Demonceau, F. Cerfontaine, J.-P. Jaspart, Resistance of steel and composite connections under combined axial force and bending including group effects: analytical procedures and comparison with laboratory tests, J. Constr. Steel Res. 160 (2019) 320–331.

[39] S. Xiang, Y. He, X. Zhou, Performance assessment of steel parking structure columns subjected to frontal collision based on reduced vehicular models, Eng. Struct. 265 (2022), 114517.

[40] GB 50017–2017, Standard for Design of Steel Structures, China Architecture & Building Press, Beijing, 2017 (in Chineses).

[41] BS EN 1991-–1-7:2006, Eurocode 1: Actions on Structures — Part 1–7: General Actions — Accidental Actions, European Committee for Standardization, Brussels, Belgium, 2006.

[42] BS EN 14010: 2003 +A1: 2009, Safety of Machinery — Equipment for Power Driven Parking of Motor Vehicles — Safety and EMC Requirements for Design, Manufacturing, Erection and Commissioning Stages, European Committee for Standardization, Brussels, Belgium, 2009.